Conditioning-controlled retrieval of broadband land surface temperature and emissivity from paired ground-based longwave irradiance measurements

Collins Mito

Department of Physics, Faculty of Science and Technology, University of Nairobi, Nairobi, P.O. Box 30197-00100, Kenya

~~*Correspondence to*~~Correspondence to: Collins Mito (collins@uonbi.ac.ke)

Abstract. Accurate retrieval of land surface temperature (~~LST~~T_s) from broadband longwave radiometric measurements is ~~fundamentally~~ limited by the nonlinear coupling between surface emissivity (ϵ) and temperature, ~~which can render the inverse problem weakly observable under low irradiance contrast . We present a~~ particularly when the available radiative contrast provides insufficient information to distinguish their contributions. A conditioning-controlled ~~retrieval methodology that estimates broadband surface emissivity and LST directly from~~ framework is presented for jointly retrieving broadband ϵ and T_s directly from high-temporal-resolution paired ground-based upwelling ~~and downwelling~~ (L) and downwelling (l) longwave irradiance measurements~~acquired at high temporal resolution. The approach combines adaptive temporal pairing constrained by a~~, without requiring externally prescribed emissivity as a retrieval input. The framework constructs a local population of candidate temporal pairs and combines quasi-steady ~~apparent surface temperature criterion with a fixed-iteration Newton inversion, and explicitly diagnoses inversion stability through Jacobian strength, residual magnitude, and observed convergence order. A formal uncertainty propagation framework is developed for both independent and correlated irradiance error structures, enabling decomposition of irradiance-driven and emissivity-driven temperature uncertainty . The method is evaluated using 39 datasets from four Surface Radiation Budget (SURFRAD) Network sites spanning diverse atmospheric conditions. The Newton inversion exhibited stable and well-conditioned behaviour across all cases,~~ thermal-state screening, numerical and physical admissibility, explicit irradiance-identifiability testing, uncertainty- and information-aware progressive pair selection, physical-state-dependent reciprocal emissivity treatment, fixed eight-update Newton-Raphson refinement, and ~~retrieved surface temperatures agreed with independent in-situ measurements with a root mean square error of 0.54 Kand a~~ correlated uncertainty propagation. Field evaluation used 637 datasets from nine SURFRAD and BSRN stations spanning vegetated, mixed, and bare/desert environments. Five datasets lacked the required finite initial irradiances, leaving 632 usable cases, all of which produced final finite retrievals; 628 reached the stable-centre selection criterion and four required the prescribed fallback pathway. Across the 632 field cases, retrieved T_s had a bias of -0.162 K, mean absolute error ~~of 0.47 K, consistent with propagated uncertainty estimates. Results demonstrate that reliable broadband LST retrieval can be achieved without externally prescribed emissivity products when inversion conditioning and measurement uncertainty are explicitly incorporated into the~~

~~retrieval design~~(MAE) of 0.432 K, root-mean-square error (RMSE) of 0.558 K, and $R^2 = 0.9984$ relative to the ground-based validation-reference temperature. A complementary physics-based known-truth experiment independently prescribed ϵ_{true} and $T_{s,true}$ for 6000 scenes spanning $0.85 \leq \epsilon_{true} \leq 0.99$. In the noiseless experiment, 5924 scenes (98.73 %) yielded successful retrievals; among successful cases, emissivity bias, MAE, and RMSE were 0.0313, 0.0491, and 0.0658, respectively, while the corresponding T_s values were -0.335, 1.307, and 3.213 K. Retrieval errors increased toward the lowest-emissivity regime, identifying low-emissivity conditions as the most demanding part of the tested retrieval space. The combined field and known-truth results demonstrate that broadband emissivity and surface temperature can be jointly retrieved from paired longwave irradiance observations when radiative observability and physical applicability are explicitly conditioned before nonlinear inversion.

1 Introduction

Land surface temperature (~~LST~~T_s) is a fundamental variable in studies of surface energy balance, land-atmosphere coupling, hydrology, and climate variability (~~Li~~ Dash et al., ~~2013; Wan~~ 2002; Li et al., ~~2015~~2013, 2023; Wan, 2014). Accurate estimation of ~~LST is essential for understanding~~ T_s is important for quantifying surface fluxes, diagnosing land-atmosphere feedbacks, and evaluating ~~satellite-based thermal infrared products. While~~ thermal infrared satellite products. Although satellite observations provide ~~global~~ broad spatial coverage, ground-based radiometric networks remain ~~indispensable for algorithmic~~ essential for algorithm development, physical interpretation, and validation because they provide continuous longwave measurements at high temporal resolution.

~~Broadband longwave irradiance measurements offer a direct link between surface state and observed radiation, but converting these to temperature is non-trivial due to emissivity coupling. Most existing approaches for deriving surface temperature from SURFRAD observations prescribe surface~~ At the land-atmosphere interface, measured broadband upwelling longwave irradiance contains both surface thermal emission and reflected atmospheric downwelling irradiance. Conversion of this measurement to T_s is therefore inseparable from broadband surface emissivity. In a single broadband observation, emissivity and temperature are nonlinearly coupled and cannot generally be retrieved independently without additional information. Even when multiple observations are available, the inverse problem can remain weakly constrained if the observations provide insufficient radiative contrast. Small measurement perturbations may then produce disproportionately large changes in retrieved emissivity and, through the emissivity correction, in surface temperature. The problem is therefore one of both radiative physics and parameter observability.

More generally, if N temporal observations are considered while emissivity is treated as common but surface temperature is allowed to vary, the system contains N radiometric equations for N temperature states plus one common emissivity—that is, N equations for N+1 unknowns before additional physical information is introduced. The quasi-steady, physical-admissibility, irradiance-identifiability, and population-information constraints therefore address this structural underdetermination, whereas low irradiance contrast is a separate factor that can further weaken conditioning by reducing measurement sensitivity.

A common approach in ground-based T_s estimation is to prescribe emissivity externally, ~~typically using~~ often from satellite-derived narrowband emissivity products ~~from sensors such as MODIS (~~that are subsequently converted to broadband values. Such products have been widely used with SURFRAD measurements (Li et al., 2014; Zhang et al~~(2016); Wang et al(~~., 2016; Wang et al., 2019~~); Li et .al(2014)).These emissivities are often obtained from coarse resolution, temporally composited products and then converted into broadband values. While widely used, this practice introduces multiple sources of uncertainty , including~~). However, externally prescribed emissivities can introduce additional uncertainty through spatial mismatch between ~~instantaneous in situ observations and multi-day composites~~a point-scale radiometric observation and a satellite pixel, temporal mismatch between an instantaneous surface state and temporally composited emissivity products, and spectral mismatch between narrowband ~~emissivities and broadband irradiance exchange~~ and broadband emissivity (Gillespie et al., 1998; Hulley and Hook, 2011; Li et al., 2019). ~~In addition, emissivity uncertainty is rarely propagated explicitly, and the numerical conditioning of the resulting surface temperature estimate is seldom examined~~These limitations motivate methods that can infer broadband emissivity directly from the longwave measurements themselves rather than requiring emissivity as an external retrieval input.

~~From an inverse-problem perspective, the challenge is more fundamental. Broadband upwelling irradiance depends jointly on surface temperature, surface emissivity, and downwelling atmospheric irradiance. With a single observation, emissivity and temperature are inseparable even with multiple observations, the problem may remain ill-conditioned if the observations are poorly chosen. As a result, emissivity retrieval can become numerically unstable, leading to amplified uncertainty in surface temperature estimates. Despite this, many previous studies focus primarily on retrieval accuracy while giving limited attention to convergence behavior, conditioning, and uncertainty structure.~~

~~The high temporal resolution of SURFRAD measurements provides an opportunity to address this limitation~~High-temporal-resolution ground-based longwave observations provide one possible source of the additional information required for such a retrieval. Over sufficiently short intervals, broadband surface emissivity can reasonably be treated as invariant and the thermodynamic surface state may change only gradually, while atmospheric forcing and the measured longwave irradiances continue to vary. Paired observations can therefore provide two radiative states for the same emissivity and improve the potential observability of the emissivity-temperature system. Ground-based ~~broadband longwave radiometric~~ networks such as SURFRAD are particularly suitable for investigating this approach because they provide continuous, ~~well calibrated measurements of~~ well-calibrated upwelling and downwelling longwave ~~radiation~~ measurements at high temporal resolution (Augustine et al., 2000~~; Augustine et al.~~, 2005). ~~Over short time intervals, surface emissivity may be treated as invariant, while surface temperature can be assumed to vary slowly. Temporal pairing of irradiance measurements therefore introduces additional information that improves emissivity observability without altering the underlying physics. However, temporal paring alone~~

Temporal pairing alone, however, does not guarantee ~~a well posed inversion. Explicit attention to numerical conditioning, convergence diagnostics, and uncertainty propagation is required to ensure physically meaningful and stable solutions.~~

~~In this study, a diagnostic-driven framework for retrieving broadband surface emissivity and surface temperature directly from paired~~ that the added observation contains useful independent information. A pair may satisfy a short temporal-separation requirement yet remain weakly informative if the changes in upwelling and downwelling ~~longwave irradiance measurements is presented. The method employs adaptive temporal pairing constrained by~~ irradiance are dominated by common atmospheric forcing. Conversely, increasing the temporal separation can improve radiative contrast but can eventually violate the assumption of a quasi-steady ~~apparent surface temperature, followed by a fixed-iteration Newton inversion of emissivity. Rather than relying solely on retrieval accuracy, the approach emphasizes convergence diagnostics, Jacobian conditioning, and uncertainty decomposition. A linearized emissivity estimate is used strictly as a diagnostic tool, while the Newton solution is retained as the physically meaningful estimate. Surface temperature uncertainty is explicitly decomposed into irradiance-driven and emissivity-driven components, enabling transparent interpretation of retrieval reliability~~surface state. The relevant problem is therefore not simply how far apart two observations should be, but whether a local population of candidate observations contains enough physically distinguishable information to constrain emissivity without introducing excessive thermodynamic change.

This distinction motivates an explicit separation between thermal-state consistency, irradiance identifiability, and information sufficiency. Thermal-state consistency limits changes in apparent surface temperature over a candidate interval. Irradiance identifiability tests whether the temporal change in upwelling irradiance contains a resolvable surface-sensitive component relative to the contemporaneous change in downwelling irradiance. Information sufficiency then asks whether the local candidate population contains enough effectively independent observations for a stable emissivity state to be identified. These controls address different limitations of the inverse problem and should not be reduced to a single temporal-separation or numerical-convergence criterion.

The ~~remainder of the paper is organized as follows. Section 2 introduces the physical and conceptual background underlying broadband longwave irradiance coupling, apparent surface temperature, and emissivity observability. Section 3 presents the emissivity inversion methodology, including the irradiance model, adaptive temporal pairing, Newton inversion, convergence diagnostics, sensitivity analysis, and uncertainty propagation. Section 4 describes the experimental setup and validation framework, including data coverage, reference emissivity and temperature sources, and contextual comparison with existing SURFRAD-based approaches. Section 5 presents the results, focusing on numerical convergence behavior, conditioning diagnostics , emissivity retrieval performance, surface temperature validation, and uncertainty decomposition. Finally, Sect. 6 summarizes the main findings and discusses the implications of the proposed diagnostics-driven framework for broadband surface temperature retrieval from ground-based radiometric observations~~numerical solution provides another layer of information but cannot substitute for radiometric observability. Newton-Raphson inversion can solve the nonlinear broadband irradiance equation once a physically meaningful initial state and informative observation pair have been established. The residual and local derivative of the nonlinear equation are useful diagnostics of numerical consistency and sensitivity, but small residuals or completed iterations do not demonstrate that arbitrary observation pairs are well conditioned. Numerical diagnostics are therefore most meaningful when interpreted after physical and information-based screening rather than as the sole basis for retrieval acceptance.

~~2 Physical and conceptual background~~

A further issue concerns the physical state used to initialize the nonlinear emissivity inversion. Algebraically related emissivity representations can correspond to different local radiative states and should not necessarily be applied uniformly across all observations. A physically conditioned retrieval should therefore consider not only whether sufficient information is available, but also whether the local longwave state supports the emissivity transformation being applied. This motivates a retrieval architecture in which temporal information selection and physical-state applicability are evaluated before the final nonlinear refinement.

~~Broadband longwave irradiance exchange between the surface and atmosphere is governed by surface emissivity , surface temperature, and atmospheric emission (Rodgers, 2000; Li et al. , 2013). At the land-atmosphere interface,~~ Uncertainty propagation is similarly important but requires careful interpretation. Formal propagation from irradiance uncertainty through the emissivity inversion provides a measure of local measurement sensitivity and enables the contributions of irradiance and emissivity uncertainty to T_s uncertainty to be separated. Such propagated uncertainties are valuable diagnostics of the ~~upwelling longwave irradiance measured above the surface represents the combined contribution of surface emission and reflected downwelling atmospheric irradiance, while the downwelling component captures atmospheric emission incident on the surface. In broadband form, these quantities are commonly expressed through the Stefan-Boltzmann framework, in which surface emissivity and surface (skin) temperature jointly govern the emitted irradiance flux. However, land surface temperature retrieval remains fundamentally limited by emissivity observability and irradiance coupling (Li et al., 2023; Dash et al., 2002)~~retrieval geometry, but they are not automatically calibrated confidence intervals. Independent known-truth experiments are required to determine whether the nominal uncertainty magnitudes adequately represent actual retrieval error across different emissivity regimes.

~~A fundamental challenge arises because broadband irradiance measurements alone do not uniquely constrain both surface emissivity and surface temperature. For a single observation, the two quantities are nonlinearly coupled, leading to an underdetermined and potentially ill-conditioned inverse problem. Small perturbations in emissivity can induce disproportionately large changes in retrieved temperature, particularly under conditions of high emissivity or strong atmospheric downwelling irradiance . This coupling has motivated many previous studies to rely on externally prescribed emissivity values, often derived from satellite products, when converting in situ broadband irradiance to land surface temperature.~~

~~An alternative perspective is provided by the concept of apparent surface temperature, defined directly from the measured upwelling irradiance under the assumption of unit emissivity. Although this apparent temperature does not represent the true physical surface temperature (Norman et al., 1995; Li et al. , 2013), it is fully observable from irradiance measurements and provides a physical meaningful upper bound on the actual surface temperature. Importantly, variations in apparent temperature over short intervals primarily reflect changes in radiative forcing rather than abrupt changes in surface thermodynamic state~~Validation of broadband emissivity presents an additional challenge. Field surface-temperature references can be constructed from ground-based longwave irradiances using externally specified emissivity, but such references are not fully independent of the radiometric measurements used by the retrieval. They provide realistic field validation of the combined retrieval behaviour, but they do not provide independent broadband emissivity truth. Direct evaluation of emissivity retrieval accuracy therefore requires a complementary experiment in which both emissivity and temperature are prescribed independently before the longwave observations are generated.

~~High temporal resolution broadband longwave observations offer an opportunity to exploit this property. Over sufficiently short time windows (60 seconds for SURFRAD), surface emissivity can be assumed invariant and the true surface temperature quasi-steady, while atmospheric irradiance conditions evolve enough to introduce measurable contrast in upwelling and downwelling irradiance. Temporal pairing of broadband irradiance measurements therefore introduces additional physical information that improves emissivity observability without modifying the underlying irradiance physics.~~

~~However, the use of temporal information alone does not guarantee a well-posed inversion. Poorly chosen temporal pairs can amplify temperature variability or lead to weak irradiance contrast, resulting in numerical instability and unreliable emissivity estimates. Any physically meaningful retrieval strategy must therefore incorporate explicit constraints that preserve~~ This study develops a conditioning-controlled framework for jointly retrieving broadband surface emissivity and T_s from paired ground-based upwelling (L) and downwelling (l) longwave irradiance observations. The framework constructs a local population of temporal pairs and combines quasi-steady ~~surface conditions while enhancing irradiance contrast, and must assess the conditioning of the resulting inversion.~~

~~In this study , these principles motivate a diagnostic-driven emissivity and surface temperature retrieval framework that relies solely on paired broadband upwelling~~ thermal-state screening, numerical and ~~downwelling irradiance measurements. The following section formalizes this framework through a nonlinear inversion scheme with explicit convergence diagnostics, sensitivity analysis, and uncertainty propagation, ensuring that numerical stability and physical interpretability are treated as integral components of the retrieval rather than post-hoc considerations.~~

~~3 Emissivity and surface temperature retrieval~~

physical admissibility, explicit irradiance-identifiability testing, uncertainty- and information-aware progressive pair selection, physical-state-dependent reciprocal emissivity treatment, Newton-Raphson refinement, and correlated uncertainty propagation. Information content is assessed before nonlinear inversion, and the selected production pair is not ranked according to its emissivity value.

~~This section describes the irradiance formulation, emissivity inversion strategy, numerical diagnostics,~~ Here, “conditioning-controlled” denotes the use of physical-state, irradiance-identifiability, and ~~uncertainty propagation framework used to retrieve broadband surface emissivity and land surface temperature from paired upwelling and downwelling longwave irradiance measurements. The methodology is intentionally diagnostic-driven, emphasizing conditioning, convergence behavior, and uncertainty control rather than accuracy alone.~~

~~3.1 Irradiance model~~

~~Surface thermal emission is modelled using a two-component broadband longwave irradiance balance that accounts explicitly for surface emissivity and atmospheric downwelling irradiance. Assuming that sensor measures hemispherically integrated longwave irradiance, the upwelling longwave irradiance measured above the surface at a given time is expressed as:~~

~~, (1)~~

~~where: is the measured upwelling longwave irradiance (); is the Stefan-Boltzmann constant ();is the absolute surface temperature ();is the downwelling atmospheric longwave irradiance (), and is the broadband surface emissivity. Equation (1) assumes hemispherical emission and reflection and is appropriate for broadband longwave irradiance exchange at the surface. Rearranging Eq. (1) yields which highlights that emissivity and surface temperature are intrinsically coupled through the emitted term.~~

~~To find the surface temperature from the other known measured quantities, we algebraically isolatein Eq. (1) to get emissivity-corrected surface temperature:~~

~~, (2)~~ information-sufficiency controls to determine which observation geometry is passed to the nonlinear solver; it does not refer solely to a numerical condition-number threshold.

The framework is evaluated using two complementary validation strategies. The field experiment contains 637 source datasets from nine SURFRAD and BSRN stations spanning vegetated, mixed, and bare/desert environments; 632 datasets contain the required initial irradiances and form the final field-validation population. A separate physics-based experiment contains 6000 independently prescribed truth scenes spanning $0.85 \le \epsilon_{true} \le 0.99$, with exactly 2000 scenes in each of three predefined emissivity regimes. The synthetic observations are generated using the exact forward broadband longwave relation, and the same truth scenes are evaluated under noiseless and production-noise conditions without using the validation results to retune the retrieval.

~~Equation (2) is widely used in surface energy balance studies when emissivity is prescribed. However, when emissivity is unknown, Eq. (~~The study addresses three related questions: (i) can a local population of paired longwave observations be screened and selected in a way that provides stable emissivity information without prescribing a fixed temporal separation; (ii) how do observable radiative contrast, local nonlinear sensitivity, and propagated retrieval uncertainty relate within the accepted field population; and (iii) can the resulting retrieval recover independently prescribed broadband emissivity and surface temperature across a broadened emissivity range? Section 2 ~~) highlights the strong nonlinear coupling between emissivity and temperature. An apparent (emissivity-independent) surface temperature is also defined directly from the measured upwelling irradiance:~~

~~(~~summarizes the physical basis of broadband longwave coupling and apparent surface temperature. Section 3 ~~)~~

~~Althoughdoes not represent the true surface temperature, it provides a physically meaningful upper bound and is fully observable from irradiance measurements. The difference between this apparent temperature and the true surface temperature reflects emissivity effects. This quantity is later used as a constraint in adaptive temporal pairing.~~

~~Equation (2) illustrates three important implications. First, emissivity and temperature are inseparable from a single broadband observation, rendering the inverse problem undetermined. Second, small emissivity errors can lead to large temperature errors, particularly near. Third, at viewing altitudes above the surface, additional atmospheric terms would further complicate the relationship. In this study, the initial focus is rigorously maintained on surface ground-based broadband irradiance measurements where atmospheric transmittance effects are negligible. This choice is intentional, as it isolates the fundamental ill-conditioning caused solely by the nonlinear coupling. The diagnostic framework developed is, however, structurally extensible to these more complex radiative transfer scenarios, as discussed in Sect. 6.~~

~~3.2 Newton inversion~~

~~This section describes the formulation of the Newton inversion, the initialization strategy, and the numerical behavior of the iterative solution. Emphasis is placed on ensuring physical consistency, numerical stability, and diagnostic transparency rather than on enforcing convergence through arbitrary stopping criteria. The subsections that follow detail the construction of the nonlinear objective function, the treatment of emissivity-temperature coupling, and the diagnostics used to assess convergence, conditioning and solution reliability.~~

~~3.2.1 Broadband emissivity retrieval~~

~~Broadband emissivity is retrieved by solving an implicit nonlinear equation derived from the two time irradiance model. Equation (2) can be written in a more convenient form by introducing the emissivity-induced temperature correction:~~

~~, (4)~~

~~where:~~

~~, (5)~~

~~The emissivity-induced temperature correctionis defined as the difference between the apparent (blackbody) surface temperatureand the emissivity-corrected surface temperature. Expressed directly in terms of measured upwelling and downwelling irradiances, is given by Eq. (5). This formulation ensures dimensional consistency, vanishes in the blackbody limit (), and is fully~~

~~consistent with the numerical implementation. Rearranging Eq. (~~presents the conditioning-controlled retrieval methodology. Section 4 describes the field and physics-based known-truth validation experiments. Section 5 ~~) yields:~~

~~(~~presents the results and discussion, and Sect. 6 ~~)~~

~~To reduce sensitivity to absolute calibration errors and slowly varying atmospheric conditions, the inversion uses two irradiance measurements () acquired within a short interval () where emissivity is assumed invariant~~summarizes the principal findings and limitations.

~~Henceforth, upwelling irradiance at timeis denoted, and downwelling irradiance asto simplify the two-time notation. The emissivity-induced temperature correction is then approximated as:~~

~~, (7)~~

2 Physical and conceptual background

~~where:~~

2.1 Broadband surface-atmosphere longwave coupling

Broadband longwave irradiance exchange at the land-atmosphere interface is governed principally by surface temperature, surface emissivity,

~~Substituting this approximation into Eq. (6) yields an implicit nonlinear equation in emissivity:~~

~~, (8)~~

~~where:~~

~~Equation (8) contains emissivityboth explicitly and implicitly through, and therefore must be solved numerically. The root is obtained using the Newton-Raphson method (Ortega and Rheinboldt~~and atmospheric downwelling emission (Rodgers, 2000~~; Nocedal and Wright, 2006):~~

~~, (9~~). For an opaque surface and for measurements sufficiently close to the surface that additional atmospheric path terms between the surface and radiometer can be neglected, the measured upwelling irradiance L can be written as

~~where:is the iteration index, and is the number of iterations. The derivative of Eq. (8),is computed analytically using the chain and product rules to get:~~

$$L = \epsilon\sigma T_s^4 + (1-\epsilon)l. \tag{1}$$

~~, (~~Here, l is the measured downwelling longwave irradiance, is broadband surface emissivity, T_s is physical surface temperature, and $= 5.670374419 \times$ 10~~)~~

~~where:~~

~~For this diagnostic analysis, a fixed, small maximum number of iterations,is used instead of a dynamic convergence tolerance. This deliberate choice allows for transparent, post-hoc analysis of the convergence rate (), residual magnitude, and Jacobian strength across every case, which is central to diagnosing solution stability (Sect. 3.3). Solutions are constrained to the physically meaningful rangeThis fixed iteration count, , should be distinguished from the adaptive temporal adjustment count, , reported in Table 1 and Figure 4, which reflects data selection effort. It should be noted that for an operational implementation, a dynamic stopping criterion would be employed, as discussed in Sect. 6.~~

~~3.2.2 Determination of the initial (linearized) emissivity estimate~~

~~The convergence and stability of the Newton-Raphson method are inherently sensitive to the choice of the initial guess. For the nonlinear irradiancebalance defined in Eq. (8), a robust initialization strategy ensures the iteration begins within the basin of attraction of the physical root. While it is assumed that only one physical meaningful root exists within the domain, a robust initialization strategy is required to ensure the iteration begins within the basin of attraction of this root.~~

~~A physically motivated initial guess is derived via a first-order Taylor expansion of the fourth-root terms:~~

~~, (11)~~

~~Substituting this linear approximation in the governing equation,~~ $^{-8}$ W m^{-2} K^{-4} is the Stefan-Boltzmann constant. The first term in Eq. (~~8) , allows for the algebraic isolation of emissivity. By applying a binomial expansion and truncating at the first-order term, we obtain the linearized emissivity estimate:~~

1) represents thermal emission by the surface, whereas the second represents the reflected fraction of atmospheric downwelling irradiance. If is externally specified, Eq. (~~12)~~

~~The quantities,,, and are algebraic combinations of the measured upwelling () and downwelling () irradiances. Specifically, represents the net surface-emitted irradiance at the first time step; the coefficientarises from a first-order Taylor expansion of the fourth-root temperature correction with respect to emissivity and is defined as; the termrepresents an effective irradiance contrast between upwelling and downwelling fields and is given by; the quantityis ; and.~~

~~The linearized emissivity provides a physically motivated initial guess for Newton's method. Importantly, is retained strictly as a diagnostic and~~

~~initialization aid. Its value provides a crucial baseline: it represents the solution obtainable if the system were purely linear or if the non-linear coupling terms were ignored. As demonstrated in Sect. 3.5.1, its uncertainty diverges dramatically under conditions of weak irradiance contrast where the linearization assumption breaks down. This divergence, rather than the magnitude ofitself, serves as a critical diagnostic confirming the necessity of the full Newton inversion and its associated Jacobian control~~1) can be solved directly for T_s. If both T_s and are unknown, however, a single observation provides one radiometric equation for two coupled surface variables.

2.2 Apparent surface temperature as an observable state diagnostic

~~Once the broadband emissivityis retrieved via the Newton-Raphson method, the final corrected surface temperatureis computed by applying the correction termto the mean apparent surface temperature. In this framework, the mean apparent (blackbody) surface temperatureis derived from the upwelling irradiances at the two observation times~~Taking the surface as a unit-emissivity emitter provides an observable radiometric temperature directly from the measured upwelling irradiance:

$$T_s{}' = \left(\frac{L}{\sigma}\right)^{1/4}. \tag{2}$$

Defining the equivalent radiative temperature of the downwelling irradiance as $T_l = (l/\sigma)^{1/4}$, Eqs. (~~13)~~ 1) and (2) give

~~This mean apparent temperature serves as the observable baseline for the retrieval. The final physically corrected surface temperature is then obtained by subtracting the emissivity-induced correction term from this baseline:. By using the mean of the two irradiance measurements, the retrieval becomes less sensitive to instantaneous instrument noise and transient micro-scale fluctuations.~~

$$T_s{}'^4 = \epsilon T_s^4 + (1-\epsilon) T_l^4. \tag{3}$$

~~To ensure the validity of the two-time irradiance model, candidate irradiance pairs must satisfy the~~ Thus, $T_s{}'$ represents an emissivity-weighted radiometric state formed from the physical surface and atmospheric longwave contributions. It should not in general be interpreted as the physical T_s, nor as a universal upper or lower bound on T_s. Its principal value here is diagnostic: because $T_s{}'$ is directly observable, changes in $T_s{}'$ between two nearby observations indicate whether the combined surface radiative state has changed appreciably.

The retrieval therefore uses the difference ${T_s}'(t_2) - {T_s}'(t_1)$ as a quasi-steady ~~apparent temperature constraint:~~ screening variable rather than assuming that temporal proximity alone guarantees thermal stability.

~~(14)~~

2.3 Temporal pairing, identifiability, and conditioning

~~This constraint serves a critical dual purpose in the diagnostic framework. First, it enforces physical consistency. The retrieval assumes that the surface emissivity is invariant and the true skin temperaturevaries slowly over the interval. By limiting the change in apparent (blackbody) temperature to a small threshold (e.g.,), the algorithm filters out periods of rapid thermal transition, such as those caused by cloud shadows, sudden wind gusts, or the onset of precipitation. Second, it optimizes numerical conditioning. If the change in apparent temperature is too large, thecoupling in the Newton Jacobian becomes non-stationary, leading to emissivity-driven temperature errors. By enforcing Eq. (14), the algorithm ensures that~~ For two observations, the same emissivity can be written in the two radiative balances $L_1 = \epsilon\sigma T_{s,1}^4 + (1-\epsilon)l_1$ and $L_2 = \epsilon\sigma T_{s,2}^4 + (1-\epsilon)l_2$. Over a sufficiently short interval, broadband emissivity can be treated as invariant. If the physical surface-temperature change is also sufficiently limited, the ~~observed irradiance differences are primarily driven by the contrast between surface emission and atmospheric downwelling irradiance rather than shifting thermodynamic state. This makes Eq. (14) a fundamental diagnostic filter that precedes the inversion, ensuring that only well-posed data pairs are passed to the Newton solver~~two observations provide additional information through their differing radiative states.

~~3.3 Newton diagnostics for emissivity inversion~~

~~Because convergence of a nonlinear solver does not , by itself , guarantee physical observability or numerical reliability, the emissivity inversion is evaluated using a set of complementary Newton diagnostics. These diagnostics quantify irradiance consistency, local curvature of the inversion, and convergence behavior, allowing well-conditioned solutions to be distinguished from cases where convergence occurs under weak emissivity observability. The following subsections describe the residual magnitude, Jacobian strength, observed order of convergence, and iteration count diagnostics, and explain how they are interpreted collectively to assess the stability and physical reliability of the retrieved emissivity.~~

~~3.3.1 Residual magnitude~~

~~At the final Newton iteration, the residual magnitude, defined in Eq. (8), quantifies the degree to which the irradiance balance equation is satisfied by the retrieved emissivity (Tarantola, 2005; Rodgers, 2000). This diagnostic is independent of convergence rate and provides a direct measure of self-consistency between the solution and the observed upwelling and~~

~~downwelling irradiance measurements. A small residual indicates that the retrieved emissivity produces the measured irradiances within the limits of the forwarded model~~The existence of two observations does not by itself make emissivity identifiable. Define $\Delta L = L_2 - L_1$ and $\Delta l = l_2 - l_1$. If the change in L closely follows the change in l, the pair may contain little additional surface-sensitive information even though both irradiances are measured accurately. Conversely, a pair becomes more informative when the upwelling change contains a resolvable component beyond the contemporaneous downwelling change. This motivates the distinction between temporal admissibility and irradiance identifiability.

~~The residual threshold adopted in this study given by Eq. (15), is selected to be consistent with the expected magnitude of irradiance measurement uncertainty:~~

~~, (15)~~

~~Reducing the residual below this level would imply fitting noise rather than physically meaningful signal and is therefore not pursued. The residual magnitude thus serves as a necessary condition for a physically admissible solution, ensuring that the inversion does not violate irradiance balance. However, a small residual does not guarantee that the emissivity is well constrained. In particular, Newton's method may converge to a solution with a small residual in regions where the forward model is weakly sensitive to emissivity, leading to large uncertainty despite apparent convergence. For this reason, residual-based diagnostics must be interpreted in conjunction with Jacobian-based conditioning metrics, which are discussed in the following subsection.~~ Observability refers to whether the measurements contain information about the unknown surface state; irradiance identifiability refers more specifically to whether a candidate pair contains a resolvable surface-sensitive contrast relative to changes in atmospheric downwelling irradiance; and numerical conditioning describes the sensitivity of the nonlinear solution to perturbations in the measurements or state variables. These concepts are treated separately in the retrieval. Physical and radiometric information are assessed before the final nonlinear inversion, and Newton residuals and local sensitivities are interpreted as diagnostics of an already selected production state rather than as substitutes for observability.

~~3.3.2 Jacobian strength~~

3 Emissivity and surface temperature retrieval

~~The minimum Jacobian magnitude, denoted min, is defined as the smallest absolute value of the Newton Jacobian encountered during the inversion. This quantity characterizes the local curvature of the~~ The retrieval combines radiometric preprocessing, population-based candidate construction and screening, irradiance-identifiability testing, information-aware progressive pair selection, physically conditioned emissivity initialization, nonlinear ~~irradiance balance equation with respect to emissivity and directly controls the stability and uncertainty of the retrieved solution. From implicit differentiation of the governing equation we get:~~ Newton-Raphson refinement, and uncertainty propagation. The complete production sequence is summarized in Fig. 1.

~~, (16)~~

3.1 Broadband longwave formulation

~~indicating that small Jacobian magnitudes lead to large amplification of measurement uncertainty in the retrieved emissivity. Physically, a small Jacobian corresponds to a locally flat inversion surface, (Tarantola, 2005; Menke, 2012; Aster et al., 2019), implying weak sensitivity of the irradiance model to emissivity and , poor observability. The first-order uncertainty relationship expressed in Eq. (16) is mathematically exact under linearization and forms the basis for interpreting Jacobian strength as a conditioning diagnostic. Thresholds used to classify Jacobian behavior, given in~~ When emissivity is known, Eq. (~~17) are not universal constants but are instead selected relative to the observed growth of emissivity uncertainty:~~ 1) can be rearranged to give

$$T_s = \left(\frac{L-(1-\epsilon)l}{\epsilon\sigma}\right)^{1/4}. \tag{4}$$

When ϵ is unknown, Eq. (~~17)~~ 4) emphasizes the nonlinear coupling between emissivity and temperature. Apparent temperature from Eq. (2) is therefore used only as a short-term state diagnostic, not as the retrieved physical temperature.

~~This approach ensures that conditioning is assessed in a data-consistent and physically meaningful manner. Accordingly, Jacobian strength is interpreted in conjunction with uncertainty behavior rather than in isolation. This data-driven classification avoids arbitrary numerical cutoffs and provides a robust indicator of whether the emissivity retrieval is well constrained by the available irradiance information.~~

3.2 Radiometric preprocessing and candidate temporal-pair construction

~~3.3.3 Observed order of convergence~~

The measured $L(t)$ and $l(t)$ series are processed with a third-order Savitzky-Golay filter using an 11-sample frame. Missing-value flags are converted to missing values before processing. Where smoothing requires a complete local sequence, missing samples are temporarily filled by linear interpolation with nearest-value end treatment and the original missing locations are restored immediately after filtering; interpolation therefore enables smoothing but does not create valid observations at originally missing times.

~~The observed order of convergence provides a local, data-driven measure of how the Newton iteration behaves near solution (Ortega and Rheinboldt, 2000; Dennis and Schnabel, 1996) . If the iteration-to-iteration change in emissivity be defined as: . The observed convergence order is then estimated as:~~ For each field dataset, an initial network-specific time pair defines a validation midpoint t_m. The midpoint is used only as the temporal reference for the subsequent population-based search. All distinct candidate pairs (t_i, t_j), with $j > i$, are constructed subject to both endpoints lying within $\pm$10 min of t_m and to a maximum pair separation of 10 min,

~~(18)~~

$$|t_i - t_m| \leq 10\ min, \qquad |t_j - t_m| \leq 10\ min, \tag{5}$$

~~This quantity characterizes the local curvature of the objective function and is independent of the residual magnitude. As such, it provides complementary diagnostic information to residual and Jacobian based measures. In particular, the observed order of convergence reveals whether Newton's method is operating in a regime consistent with theoretical expectations or whether convergence is limited by weak curvature, noise or ill-conditioning.~~

$$0 < |t_j - t_i| \leq 10\ min. \tag{6}$$

~~This diagnosticis especially important for interpreting uncertainty behavior. Case exhibiting near-linear convergence () indicate reduced curvature and increased sensitivity to measurement noise, while values approaching quadratic convergence reflect well-conditioned local behavior. Conversely, sub-linear convergence signals poor observability and limited physical interpretability of the retrieved emissivity. Based on these considerations, Eq. (19) defines diagnostic thresholds used to classify convergence behavior:~~ The 10-min interval defines the maximum search geometry rather than a prescribed production separation. The actual search proceeds progressively through radii of 1, 2, ..., 10 min.

3.3 Physical, numerical, and irradiance-identifiability screening

~~These classifications follow directly from Newton convergence theory and are independent of the specific radiative transfer application, making the observed convergence order a robust and general indicator of numerical reliability.~~ All four irradiances L_1, l_1, L_2, l_2 must be finite. A candidate must also satisfy the quasi-steady apparent-temperature condition

~~3.3.4 Number of Newton iterations~~

$$|T_s{}'(t_2) - T_s{}'(t_1)| \leq 1.0\ K. \tag{7}$$

~~The number of Newton iterations required for convergence provides useful but limited diagnostics information when considered in isolation. Iteration count does not, by itself, indicate whether convergence is physically meaningful or numerically well-conditioned. A small number of iterations may occur in both strongly and weakly constrained problems, while a larger number of iterations does not necessarily imply instability~~Equation (7) limits thermodynamic-state change; satisfying this criterion alone, however, does not establish that the inverse problem is sufficiently observable.

~~For this reason, iteration count is interpreted jointly with Jacobian strength and the observed order convergence. Together, these diagnostics distinguish rapid convergence driven by strong local curvature from apparent convergence occurring in flat or weakly sensitive regions of the objective function. The iteration based diagnostic flag defined in Eq. (20) reflects this combined interpretation rather than treating iteration count as a standalone measure of performance.~~ For each surviving pair, introduce the intermediate quantities

~~(20)~~

$$N = L_1 - l_1, \tag{8}$$

~~In the present framework, iteration count is therefore used as a supporting indicator of numerical behavior, complementing residual, Jacobian, and observed order of convergence diagnostics to provide a complete assessment of inversion stability and conditioning.~~

$$C_1 = \tfrac{1}{4} l_1^{-3/4}, \qquad C_2 = \tfrac{1}{4} l_2^{-3/4}, \tag{9}$$

~~3.3.5 Combined diagnostic logic~~

$$M = \tfrac{1}{2}\left((L_1 - l_1)\, C_1 + (L_2 - l_2)\, C_2\right), \tag{10}$$

~~Newton convergence in this study is evaluated using a complementary set of diagnostics: residual magnitude, Jacobian strength, observed order of convergence, and iteration count. Together, these measures assess irradiance~~

~~self-consistency, emissivity observability, and numerical conditioning of the inversion. Each diagnostic targets a distinct failure mode and cannot, on its own, guarantee physical reliability.~~

$$J = L_1^{1/4} - \frac{1}{2}\left(L_1^{1/4} + L_2^{1/4} - l_1^{1/4} - l_2^{1/4}\right), \tag{11}$$

and $D = J^4 - l_1$, the candidate linear emissivity is

~~Solutions exhibiting small residuals but weak Jacobian strength or sub-linear convergence behavior are identified as ill conditioned and are consistently associated with inflated emissivity uncertainty. Such cases indicate convergence driven by flat or weakly sensitive regions of the objective function rather than by robust physical information. The combined diagnostic logic therefore distinguishes between convergence that reflects genuine emissivity observability and convergence that occurs despite poor conditioning.~~

$$\epsilon_{lin} = \frac{N - 4MJ^3}{D}. \tag{12}$$

~~Based on the diagnostic flag scheme defined above, a solution is considered physically reliable when the combined criteria in Eq. (21) are satisfied. These criteria provide data-driven bounds that distinguish well-conditioned from weakly conditioned inversions within the context of SURFRAD instrumentation noise levels. The diagnostics are used to interpret solution reliability and uncertainty behavior, rather than to enforce hard rejection of results:~~ Numerical screening then uses the relative denominator-conditioning measure

~~(21)~~

$$\kappa_D = \frac{\max(|J^4|, |l_1|)}{|D|}, \tag{13}$$

~~Although the form and interpretation of these diagnostics are well established in inverse-problem~~ and ~~numerical-analysis frameworks, their numerical thresholds depend on problem scaling and measurement uncertainty. In this study, thresholds were selected based on observed transitions in emissivity uncertainty growth and Newton convergence behavior, ensuring consistency with the data characteristics and the underlying irradiance physics~~candidates with $\kappa_D > 10^6$ are excluded. The resulting linear estimate must additionally satisfy $0 < \epsilon_{lin} < 1$; no clipping and no empirical lower emissivity bound are imposed.

~~3.4 Sensitivity analysis~~

~~To understand how irradiance measurements, emissivity, and surface temperature interact with the inversion, a formal sensitivity and uncertainty~~

~~analysis is performed. Sensitivity analysis quantifies how small perturbations in the measured irradiances propagate through the retrieval, revealing the mechanisms that control emissivity and temperature observability. Uncertainty propagation then translates instrument-level irradiance uncertainty into physically interpretable uncertainty bounds on the retrieved emissivity and surface temperature. Together, these analyses clarify the conditioning of the inversion, explain diagnostic behavior, and provide the theoretical basis for the uncertainty estimates reported in the results section.~~

~~This section examines how perturbations in broadband upwelling and downwelling longwave irradiance measurements influence (i) the linearized emissivity, (ii) the Newton-retrieved emissivity, and (iii) the corrected surface temperature. The objective is to identify dominant sensitivity pathways and physical regimes, independent of numerical convergence.~~ Irradiance identifiability is evaluated independently of the emissivity value. With $\Delta L = L_2 - L_1$ and $\Delta l = l_2 - l_1$, the production condition is

~~3.4.1 Sensitivity of the initial (linearized) emissivity estimate~~

$$|\Delta L| > |\Delta l|. \tag{14}$$

~~The sensitivity of the linearized emissivity estimateis examined by performing a total differentiation of its governing algebraic expression derived in Sect. 3.2.2. This analysis identifies the physical and numerical pathways through which small fluctuations in measured longwave irradiance propagate into the initial estimate. Applying the total differential to~~ Under Eq. (~~12) yields:~~

~~(22)~~

~~This expression reveals three distinct sensitivity pathways that characterize the behavior of the linearized estimate:~~

~~The termrepresents sensitivity arising directly from perturbations in the irradiance contrast at the first time step. This contribution increases as surface-emitted irradiance decreases. Under humid conditions, where~~ 14), the temporal change in measured upwelling irradiance must exceed the contemporaneous change in atmospheric downwelling irradiance~~can approach the upwelling component, this sensitivity is amplified. This pathway is local to first measurement time and is independent of the second irradiance observation; The term depends on both measurement times through the quantitiesand. Sensitivity increases when the temporal irradiance contrast is weak, i.e. , whenis small. This pathway explicitly couples emissivity to surface temperature variability, such that even small irradiance perturbations at either time can propagate strongly when temporal contrast is limited; The final term, proportional to, represents sensitivity associated with the conditioning of the denominator. Since, small values of or large atmospheric contributionscan~~

~~drivetoward zero. Under typical observational conditions, characterized by humid atmospheres and weak short-term irradiance contrast, this pathway dominates and can lead to extreme sensitivity amplification.~~ . This criterion therefore tests for a resolvable surface-sensitive radiative contrast rather than merely reflecting atmospheric forcing.

~~The key implication of this analysis is that the linearized emissivity estimate is structurally sensitive under standard observational conditions. Although it may yield emissivity values close to Newton solution, its sensitivity behavior is dominated by conditioning effects rather than physical robustness. Consequently, the linearized emissivity should be interpreted strictly as a diagnostic initialization and not as a physical reliable emissivity estimate.~~

3.4 Information-aware progressive temporal-pair selection

~~3.4.2 Sensitivity of Newton-retrieved emissivity~~

Candidate pairs satisfying Sect. 3.3 are evaluated progressively over temporal radii $r = 1, 2, \ldots, 10$ min. At radius r, only identifiable candidates whose midpoint lies within r min of t_m and whose temporal separation does not exceed r are included.

~~The emissivityis obtained by solving the implicit nonlinear equation:~~ For candidate j, the uncertainty of ϵ_{lin} is propagated from the four irradiances using

~~, (23)~~

$$\sigma^2_{\epsilon,j} = \mathbf{g}_j^{\mathsf{T}} \mathbf{C}_y \mathbf{g}_j, \tag{15}$$

where ~~denotes the measured upwelling and downwelling longwave irradiances. Because the solution satisfies, application of the implicit function theorem yields the total differential:~~

~~(24)~~

~~This gives the emissivity sensitivity to irradiance perturbations as:~~ $\mathbf{g}_j = \nabla_{\mathbf{y}} \epsilon_{lin}$ for $\mathbf{y}_j = (L_1, l_1, L_2, l_2)^{\mathsf{T}}$. The covariance matrix is

~~(25)~~

$$\mathbf{C}_y = \sigma_L^2 \begin{pmatrix} 1 & \rho_{cross} & \rho_L & \rho_{cross} \\ \rho_{cross} & 1 & \rho_{cross} & \rho_l \\ \rho_L & \rho_{cross} & 1 & \rho_{cross} \\ \rho_{cross} & \rho_l & \rho_{cross} & 1 \end{pmatrix}, \tag{16}$$

Here, ~~is the Jacobian of the inversion. Eq. (25) shows that all emissivity sensitivity is controlled by the Jacobian magnitude. When the Jacobian is small,~~

~~emissivity becomes weakly observable, regardless of how small the irradiance measurement noise may be.~~

~~From Eq. (10), the Jacobian can be decomposed into two physically distinct components. The first term represents the irradiance curvature term:~~ $_L$ denotes the standard uncertainty assigned to each longwave irradiance measurement; $_L$ and $_l$ denote the temporal correlations in the upwelling and downwelling measurements, respectively; and $_{cross}$ denotes the assumed cross-channel correlation. Candidate uncertainty contributes the baseline weight

~~(26)~~

$$w_{D,j} = \frac{1}{\sigma_{\epsilon,j}^2 + \sigma_{floor}^2}, \qquad \sigma_{floor} = 10^{-4}. \tag{17}$$

~~This term represents irradiance contrast; it is maximized under dry conditions and diminishes under humid or cloudy skies.~~ To account for the information that remains available for emissivity after allowing T_s to vary, a local two-parameter Fisher matrix is calculated. With the candidate sensitivity matrix $\mathbf{K}_j$ and the temporal upwelling covariance $\mathbf{C}_F$, the Fisher matrix is

~~The second contribution is the emissivity-temperature coupling term:~~

$$\mathbf{F}_j = \mathbf{K}_j^\top \mathbf{C}_F^{-1} \mathbf{K}_j, \tag{18}$$

~~(27)~~ Marginalizing over temperature leaves the emissivity information

~~This term arises because changes in emissivity modify the retrieved surface temperature , which then feeds back into the irradiance balance. Its sensitivity increases as emissivity approaches unity and as irradiance contrast weakens. When dominant, this coupling introduces nonlinearity and further reduces Jacobian strength rendering emissivity weakly observable.~~

$$I_{\epsilon|T,j} = F_{\epsilon\epsilon,j} - \frac{F_{\epsilon T,j}^2}{F_{TT,j}}. \tag{19}$$

The ~~full Jacobian structure may therefore be written as~~scene-wise median then normalizes the valid information values:

~~(28)~~

$$R_{F,j} = \frac{I_{\epsilon|T,j}}{median\left(I_{\epsilon|T}\right)}, \qquad w_j = w_{D,j} R_{F,j}. \tag{20}$$

~~Equation (28) shows that emissivity observability is governed by the balance between irradiance curvature and emissivity-temperature coupling. Adaptive~~

~~dt-pair selection directly influences this balance by increasing temporal separation betweenand , thereby enhancing irradiance contrast while enforcing a quasi-steady apparent surface temperature. This increases the irradiance curvature term and suppresses the relative influence of emissivity-temperature coupling.~~ If marginalized Fisher information is unavailable or non-positive, $R_{F,j} = 1$ and the uncertainty-based weight is retained. No candidate is rejected solely because of its Fisher information and no fixed Fisher-information cutoff is introduced.

~~3.4.3 Sensitivity analysis of the retrieved surface temperature~~

At each radius, the representative local emissivity state is the weighted median of the candidate ϵ_{lin} population. Because candidate pairs overlap in time, information sufficiency is evaluated from both the number of distinct source observations and an effective pair count. A stage is information sufficient when

~~The retrieved surface temperaturedepends on emissivity, upwelling longwave irradiance, and downwelling longwave irradiance. The total differential of may be written as:~~

$$N_{distinct} \geq 4, \qquad N_{eff} \geq 2.5. \tag{21}$$

~~(29)~~ Stability additionally requires the robust emissivity centre to satisfy

~~The partial derivatives are evaluated at the converged Newton solution. Equation (29) reveals two distinct pathways: emissivity-driven sensitivity and irradiance-driven sensitivity.~~

$$|\tilde{\epsilon}_r - \tilde{\epsilon}_{r-1}| \leq 0.005, \tag{22}$$

~~The emissivity dependence enters exclusively through the temperature correction term. Differentiating Eq. (4) with respect to emissivity yields:~~ for two consecutive stage transitions. Once an information-sufficient stable stage is reached, the production pair is selected independently of its emissivity value, ranked first by midpoint proximity to the validation midpoint, then by preference for a separation of at least 2 min when otherwise tied, then by longer informative span, and finally by candidate uncertainty. If stability is not demonstrated, a prescribed fallback uses the best information-sufficient stage or, where necessary, the complete identifiable population within the 10-min search geometry.

~~(30)~~

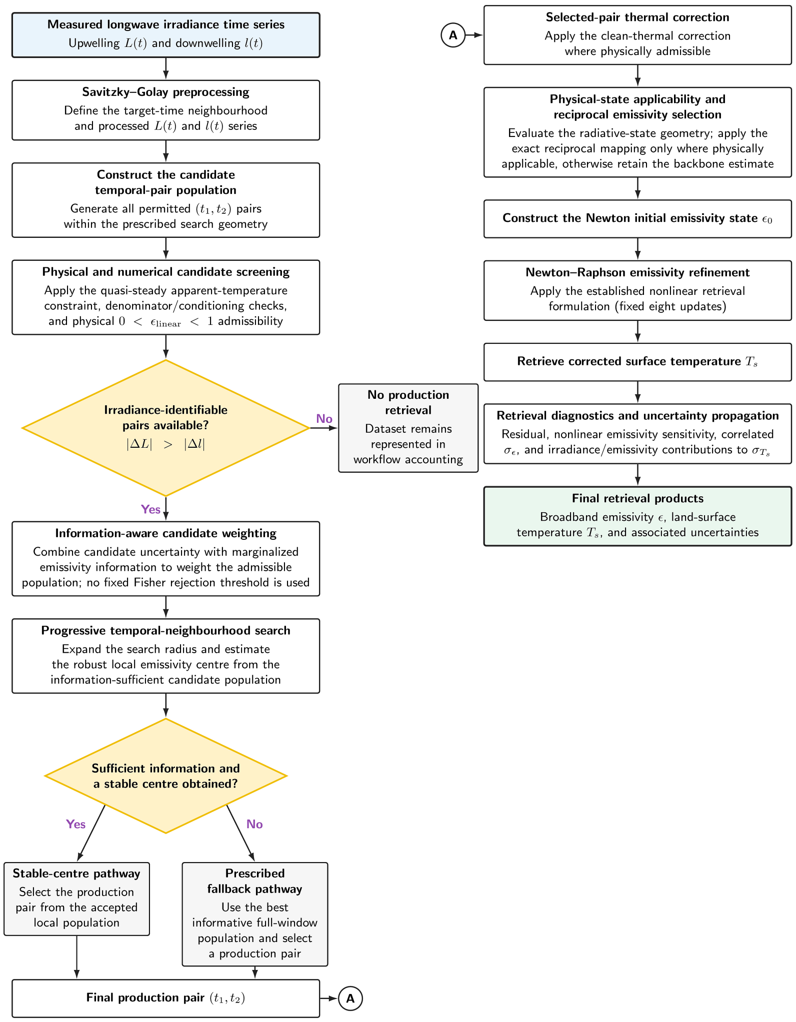

Figure 1. Conditioning-controlled production retrieval architecture, from measured $L(t)$ and $l(t)$ through candidate screening and information-aware pair selection to physical-state conditioning, Newton-Raphson refinement, surface-temperature retrieval, and uncertainty propagation. Matching A connectors indicate continuation from the final production pair to the selected-pair thermal-correction stage.

~~Equation (30) highlights several key properties. First, thedependence produces strong nonlinear amplification as emissivity approaches unity, explaining why even small emissivity errors can generate large surface temperature perturbations over high emissivity surfaces. Second, the numeratorrepresents the net surface radiant contrast; when this contrast is weak, such as under humid conditions, emissivity-driven sensitivity increases. Third,~~

~~becauseitself is controlled by the Jacobian strength of the emissivity inversion, emissivity-driven temperature sensitivity directly inherits the conditioning of the emissivity retrieval. Poor emissivity observability therefore translates into unstable temperature estimates. Emissivity-driven sensitivity dominates when emissivity is weakly constrained, downwelling irradiance is large, irradiance contrast is small, and adaptive dt-pair selection is not applied.~~

~~Irradiance-driven sensitivity arises from both terms in Eq. (29). Differentiation of the governing equation with respect to upwelling irradiance gives:~~

3.5 Selected-pair thermal correction and physical-state reciprocal emissivity treatment

~~, (31)~~

~~where~~ Once the production pair is fixed, the robust population estimate $\tilde{\epsilon}$ is retained as the production anchor. Two state-ordered linear emissivities are evaluated from the same selected pair, and the ~~first term represents the direct Planck sensitivity of the apparent surface temperature and the second term accounts for emissivity correction. Their difference reflects how emissivity modifies the irradiance response. Differentiation with respect to downwelling irradiance yields:~~

~~(32)~~ selected-pair thermal coefficient is

~~In this case sensitivity vanishes as. Downwelling irradiance affectsprimarily over low-emissivity surfaces. This term is always negative, indicating that increased atmospheric emission reduces retrieved surface temperature. In typical environmental conditions, broadband longwave irradiances are large (300-400 Wm-2) . Thescaling inherent in the model implies that sensitivity increases at lower irradiance levels, night-time and winter conditions tend to be more irradiance-sensitive than warmer daytime periods.~~

$$K_T = \frac{\Delta L}{\Delta L - \Delta l}. \tag{23}$$

~~Combing all the terms we get the full sensitivity structure of~~Applying this coefficient gives the thermal correction and corrected anchor:

~~(33)~~

~~Adaptive dt-pair selection improvesstability since it improves emissivity observability, reducesand directly suppresses emissivity-driven sensitivity. Thus, improvedstability arises from conditioning, not from smoothing or noise suppression. The sensitivity of the retrieved surface temperature is governed by the balance between emissivity-driven and irradiance-driven pathways. Improving emissivity observability through adaptive time-pair selection reduces temperature sensitivity without modifying the underlying irradiance physics.~~

~~3.5 Uncertainty propagation analysis~~

~~Broadband longwave irradiances are measured using calibrated pyrgeometers. While per-sample numerical uncertainties are not always explicitly reported, instrument accuracy is inferred from calibration traceability and standard performance assessments documented for high-quality radiometric networks. For the purpose of quantifying the final uncertainty scale, the irradiance measurement uncertainty () is set to a representative value consistent with the instrument performance standards established (Augustine et al. , 2000):~~

$$\Delta\epsilon_T = K_T\left(\epsilon_{L2} - \epsilon_{L1}\right), \qquad \epsilon_T = \tilde{\epsilon} + \Delta\epsilon_T. \tag{24}$$

~~= Constant (34)~~ The correction is applied only when the ordered emissivities, denominator, and corrected result are finite and physically admissible; otherwise $\epsilon_T = \tilde{\epsilon}$.

~~This valueserves as the input measurement uncertainty benchmark for this dataset. Unlike the simplified formulation often adopted in previous studies, irradiance errors in measurements are not strictly independent. Shared calibration constants, common atmospheric forcing and short-term drift introduce correlation both within channels (between~~ The local radiative environment of the selected pair is then characterized using the pair-mean irradiances $\overline{L}$ and ~~, between~~ $\overline{l}$, the surface-sensitive contrast $\overline{A} = \overline{L} - \overline{l}$, and ~~) and across channels (between upwelling and downwelling irradiance). In this section two complementary uncertainty propagation approaches are examined: independent error propagation and correlated error propagation. Both formulations are implemented analytically and evaluated numerically using the same emissivity model. The independent case provides a diagnostic lower bound that isolates fundamental sensitivity pathways under idealized noise conditions, while the correlated case incorporates physically realistic covariance arising from shared calibration, atmospheric coherence, and cross channel coupling in longwave irradiance measurements.~~

~~3.5.1 Uncertainty propagation of the initial (linearized) emissivity~~

~~For reference, a lower-bound estimate of uncertainty is obtained by assuming that all measured components () are statistically independent and share a common instrument uncertainty. Under this assumption, first-order uncertainty propagation yields:~~

$$\overline{S}_T = \overline{l} + \frac{\overline{A}}{\epsilon_T}, \qquad R_M = \frac{(1-\epsilon_T)\overline{A}}{\epsilon_T}. \tag{25}$$

~~(35)~~ For valid surrounding observations in the same production neighbourhood, define the normalized state by

~~The formulation in Eq. (35) represents a useful diagnostic baseline but neglects physically realistic covariance effects. It is appropriate when : instrument noise dominates, calibration errors are independent and atmospheric and surface effects do not induce cross-channel coupling.~~

$$x = \frac{S-\overline{S}_T}{R_M}, \qquad S = l + \frac{L-l}{\epsilon_T}. \tag{26}$$

~~Irradiance errors may be correlated due to: shared calibration constants, common atmospheric conditions and instrument drift. A more physically consistent uncertainty estimate is obtained by accounting explicitly for correlations among the irradiance measurements. Let the gradient of the linearized emissivity with respect to the irradiance vectorbe denoted by:~~ A second characterization follows from Stefan-Boltzmann scaling. With $T_T = \left(\overline{S}_T/\sigma\right)^{1/4}$, $T_{sky} = \left(\bar{l}/\sigma\right)^{1/4}$, $t = T_{sky}/T_T$, and $G = \bar{l}/\overline{A}$, define

$$\Psi_{SB} = 2G - \left(1 + t + t^2 + t^3\right), \qquad Z = \epsilon_T \left(1 + t + t^2 + t^3\right). \tag{27}$$

The ~~emissivity uncertainty is then expressed compactly as:~~

~~, (36)~~

~~where is the irradiance covariance matrix. In practice, the covariance matrix is parameterized as:~~

~~, (37)~~

~~where:~~ framework then considers two exact reciprocal transformations:

~~is the correlation between upwelling irradiances (),~~

$$\mathcal{R}_1\left(\epsilon_T\right) = \frac{2\epsilon_T}{1+\epsilon_T}, \qquad \mathcal{R}_2\left(\epsilon_T\right) = \frac{\epsilon_T}{2-\epsilon_T}. \tag{28}$$

~~is the correlation between upwelling irradiances ()~~ A conservative backbone selector determines the default mapping: $\mathcal{R}_1$ is selected for $\epsilon_T \lesssim 0.963$ and $\mathcal{R}_2$ for $\epsilon_T \gtrsim 0.976$. Within $0.963 < \epsilon_T < 0.976$, $\mathcal{R}_1$ is selected when the outward normalized upwelling contribution is negative or the preceding normalized state satisfies $x_{before} \leq -2/5$; otherwise $\mathcal{R}_2$ is retained.

~~is the cross-channel correlation between upwelling and downwelling irradiances.~~ The backbone decision is overridden only for two specific physical-state configurations. In the Stefan-Boltzmann-negative configuration, the mapping is governed by $r_T = \left(1-\epsilon_T\right)/\epsilon_T$ relative to $r_{SB} = (1-0.96246)/0.96246$. In the reciprocal-conductance configuration, the physical substitution is applicable only when

~~This formulation naturally captures shared calibration effects, atmospheric coherence, and instrument drift.~~

$$x_{before} < -\frac{1}{6}, \tag{29}$$

~~3.5.2 Uncertainty propagation of Newton-retrieved emissivity~~

The corresponding branch criterion is

~~First, uncertainties in upwelling and downwelling longwave irradiances are assumed independent, Gaussian, and characterized by a common variance. For an emissivitydefined implicitly by a nonlinear equation, first-order uncertainty propagation for implicit functions yields:~~

$$Z < 2 + \sqrt{2}. \tag{30}$$

Outside these physically applicable configurations, the backbone mapping is retained. The selected reciprocal result becomes the initial emissivity ϵ_0 for nonlinear refinement; if a transformed result is non-finite or falls outside $0 < \epsilon_0 < 1$, the conservative fallback $\epsilon_0 = \epsilon_T$ is used.

~~whereis the variance of the residual function induced by irradiance uncertainty. The residual functiondepends on irradiance differences and emissivity-corrected irradiance terms at both times. To first order, its variance is dominated by independent irradiance contributions:~~

3.6 Newton-Raphson emissivity refinement and surface-temperature retrieval

~~, (38)~~ Starting from $\epsilon^{(0)} = \epsilon_0$, define $P_1 = L_1^{1/4}$ and $P_2 = L_2^{1/4}$. At Newton iteration k,

~~with higher-order terms involving emissivity-temperature coupling contributing additional but bounded variance for realistic irradiance values. Consequently, remains finite and directly controlled by instrument uncertainty. The uncertainty of the Newton-retrieved emissivity, under the independent structure, becomes:~~

$$M\left(\epsilon^{(k)}\right) = \frac{1}{2}\left(P_1 + P_2 - \left(\frac{L_1 - l_1}{\epsilon^{(k)}} + l_1\right)^{1/4} - \left(\frac{L_2 - l_2}{\epsilon^{(k)}} + l_2\right)^{1/4}\right). \tag{31}$$

~~(39)~~ The nonlinear residual takes the form

~~whereis~~

$$f(\epsilon) = \epsilon\left((P_1 - M(\epsilon))^4 - l_1\right) - (L_1 - l_1)\,. \tag{32}$$

Equation (32) retains the established production sign convention; the correction enters through $P_1 - M(\epsilon)$ and is not replaced by the ~~Jacobian evaluated at the Newton solution. This expression highlights the central role of the Jacobian: emissivity uncertainty is inversely proportional to local irradiance curvature.~~

~~Second, to incorporate correlated irradiance errors, the residual variance is generalized to:~~ alternative positive-sign form. The derivative is

~~, (40)~~

$$f'(\epsilon) = (P_1 - M)^4 - l_1 - 4\epsilon\,(P_1 - M)^3\,M'(\epsilon), \tag{33}$$

where ~~is the sensitivity vector of the residual with respect to the irradiance inputs. For the two-time formulation used here, the dominant contribution arises from the upwelling irradiance difference, yielding:~~

~~The correlated Newton emissivity uncertainty therefore becomes:~~

~~(41)~~

~~This formulation reduces to Eq. (39) when all correlations vanish, but more generally yields realistic uncertainty estimates when irradiance measurements are correlated.~~

~~Unlike the linearized emissivity, the Newton-retrieved emissivity uncertainty remains structurally bounded whenever the inversion is observable. As irradiance contrast weakens, the Jacobian decreases smoothly, leading to controlled and diagnostically meaningful increase in uncertainty rather than catastrophic divergence. Adaptive temporal pairing directly strengthens the Jacobian by enhancing irradiance contrast while preserving quasi-steady surface conditions, thereby suppressing uncertainty amplification.~~

~~This distinction explains the contrasting behavior observed in Figure 7: the linearized uncertainty exhibits non-physical spikes, while the Newton uncertainty remains well-behaved and interpretable across all cases. The covariance based formulation reinforces this interpretation by ensuring that uncertainty estimates reflect both instrument characteristics and the physical coupling structure of the inversion.~~

~~3.5.3 Uncertainty decomposition and interpretation for the surface temperature~~

~~This section analyzes the uncertainty structure of the retrieved surface temperature to identify the physical and numerical mechanisms that govern~~

~~retrieval reliability beyond aggregate accuracy metrics. Because surface temperature uncertainty arises from multiple interacting pathways, including irradiance measurement noise, emissivity-temperature coupling, and inversion conditioning, explicit uncertainty decomposition is required to interpret observed errors and diagnose stability. Uncertainty is therefore examined under both independent error and correlated error assumptions. Considering both formulations is essential for distinguishing structural properties of the retrieval from artifacts of simplifying assumptions and for demonstrating that the bounded uncertainty behavior of the Newton-based frameworks persists under realistic error conditions.~~

~~Using first-order Taylor expansion, the variance of the corrected surface temperature under independent errors is expressed as:~~

$$M'(\epsilon) = -\frac{1}{8}\left(\left(\frac{L_1-l_1}{\epsilon}+l_1\right)^{-3/4}\frac{L_1-l_1}{\epsilon^2}+\left(\frac{L_2-l_2}{\epsilon}+l_2\right)^{-3/4}\frac{L_2-l_2}{\epsilon^2}\right). \tag{34}$$

~~(42)~~ Newton-Raphson then advances the emissivity according to

~~The summation indexspans all irradiance inputs. Equation (42) naturally separates the total temperature uncertainty into irradiance-driven and emissivity driven components.~~

$$\epsilon^{(k+1)} = \epsilon^{(k)} - \frac{f(\epsilon^{(k)})}{f'(\epsilon^{(k)})}. \tag{35}$$

A fixed sequence of up to eight updates is applied. The sequence is interrupted if the derivative becomes non-finite or zero, or if the next emissivity is non-finite or lies outside $0 < \epsilon^{(k+1)} < 1$. The eight-update structure provides a common numerical trajectory and is not described as an empirical stopping tolerance. The ~~irradiance-driven component of surface temperature uncertainty arises from the explicit dependence ofon the measured irradiance fields. This contribution reflects the Planck law sensitivity of both the apparent surface temperature and the emissivity correction to perturbations in upwelling and downwelling longwave irradiance. Under the independent-error assumption, this component is obtained by summing the squared partial derivations ofwith respect to each irradiance input, Eqs. (31) and (32), weighted by the common irradiance uncertainty, expressed as:~~

~~(43~~Newton–Raphson formulation follows standard nonlinear root-finding practice (Ortega and Rheinboldt, 2000; Nocedal and Wright, 2006).

~~Physically, this term represents the uncertainty that would remain even if emissivity were perfectly known. Its magnitude is governed by absolute irradiance levels and irradiance contrast and tends to increase under low~~

~~irradiance conditions, such as nighttime or cold surface regimes. Importantly, this contribution is unaffected by the conditioning of the emissivity inversion and therefore provides a stable reference against which emissivity-driven effects can be evaluated.~~

~~The emissivity-driven component of the surface temperature uncertainty enters exclusively through the emissivity-induced correction term. As shown in Sect. 3.4.3, differentiation of the corrected temperature with respect to emissivity yields the sensitivity term in Eq. (30). Propagation of the independent emissivity uncertainty derived in Sect. 3.5.2, Eq. (39), then produces the emissivity-driven temperature uncertainty:~~ After the final valid update, compute the pair-mean apparent temperature as

~~(44)~~

$$T_s{}' = \frac{P_1+P_2}{2\sigma^{1/4}}, \tag{36}$$

~~This component exhibits strong nonlinear amplification due to the explicitdependence in the sensitivity expression. Consequently, even modest emissivity uncertainty can induce substantial temperature uncertainty when emissivity approaches unity or when surface-atmosphere irradiance contrast is weak. Because emissivity uncertainty itself is controlled by the Jacobian strength of the Newton inversion, this term directly reflects the numerical conditioning and physical observability of the emissivity retrieval.~~ The associated emissivity-induced temperature correction becomes

~~Combining the irradiance-driven and emissivity-driven contributions yields the total independent-error surface temperature uncertainty:~~

$$\Delta T = \frac{P_1+P_2-\left(\frac{L_1-l_1}{\epsilon}+l_1\right)^{1/4}-\left(\frac{L_2-l_2}{\epsilon}+l_2\right)^{1/4}}{2\sigma^{1/4}}. \tag{37}$$

~~(45)~~ Finally, the retrieved surface temperature follows the established convention

~~This decomposition makes explicit that surface temperature uncertainty is not governed solely by measurement noise magnitude, but by the interaction between irradiance sensitivity and emissivity observability. Under well-conditioned inversion, irradiance driven uncertainty typically dominates, while under weak irradiance contrast the emissivity-driven contribution becomes the principal source of amplification.~~

$$T_s = T_s{}' - \Delta T. \tag{38}$$

~~Adaptive temporal pairing reduces total temperature uncertainty in the independent-error framework indirectly, by improving emissivity observability and suppressing the propagated emissivity variance, while leaving the underlying irradiance measurement uncertainty unchanged. The independent error case therefore provides a physically interpretable lower bound on temperature uncertainty and establishes the reference against which the more realistic correlated-error formulation is evaluated. Because broadband longwave irradiance errors are not independent in practice, the following paragraphs extend the analysis to a correlated error formulation to assess how physically realistic covariance modifies the surface temperature uncertainty structure.~~

~~The independent-error formulation above provides a useful diagnostic lower bound on surface temperature uncertainty but neglects physically realistic correlations among broadband longwave irradiance measurements. Under correlated error, first-order uncertainty propagation yields a surface variance consisting of two additive contributions: a covariance-weighted irradiance term involving the full irradiance covariance matrix, Eq. (37), and an emissivity-driven term obtained by propagating the correlated Newton emissivity, Eq. (41). This formulation generalizes the independent-error expression, Eq. (42) and reduces exactly to it when all off-diagonal covariance terms vanish, ensuring consistency.~~

3.7 Conditioning diagnostics and uncertainty propagation

~~The irradiance-driven component of surface temperature uncertainty under correlated errors arises from the explicit dependence ofon upwelling and downwelling irradiance. The required sensitivity terms are given by the partial derivatives derived in Sect. 3.4.3, Eqs. 31~~ The final nonlinear residual is reported as $R_f = |f(\epsilon)|$, and ~~32. Unlike the independent case, these sensitivities are now weighted by the full covariance structure rather than by a single variance. Formally,~~ the ~~correlated irradiance-driven temperature uncertainty is expressed as the quadratic form:~~ minimum local sensitivity encountered over the Newton trajectory is

~~, (46)~~

$$J_{\min} = \min_k \left| f'\left(\epsilon^{(k)}\right) \right| . \tag{39}$$

~~wheredenotes the gradient of the corrected surface temperature with respect to the irradiance vector with respect to the irradiance vector evaluated at the Newton solutions, and is given by Eq. (37). Physically, this term captures how correlated perturbations in the irradiance fields propagate into surface temperature . Positive correlation between temporally adjacent upwelling irradiances reduces uncertainty in the mean apparent temperature, while cross-channel correlation modifies the effective contribution of the emissivity correction term. Depending on the sign and magnitude of the correlation~~

~~coefficients, the irradiance-driven uncertainty may be modestly reduced or enhanced relative to the independent baseline. Importantly, this contribution remains bounded and smoothly varying, as it is governed by Planck-law sensitivity rather than inversion conditioning.~~ Using the full covariance structure gives the production emissivity uncertainty

~~The emissivity-driven component of the surface temperature uncertainty under correlated errors arises from propagation of the correlated Newton emissivity uncertainty into the emissivity-induced temperature correction. The sensitivity ofwith respect to emissivity is given by Eq. (30) and is unchanged from the~~

$$\sigma_{\epsilon,corr} = \frac{\sqrt{\mathbf{a}^{\mathsf{T}}\mathbf{C}_y\mathbf{a}}}{J_{\min}}, \qquad \mathbf{a} = (1,0,1,0)^{\mathsf{T}}. \tag{40}$$

An independent-error ~~formulation. Propagation of the correlated emissivity uncertainty derived in Sect. 3.5.2,~~ limiting form is retained only as a diagnostic. Differentiating Eq. (~~41), yields the~~ 38) with respect to emissivity gives the local temperature sensitivity $\partial T_s/\partial \epsilon$, from which the emissivity-driven ~~surface temperature uncertainty:~~

~~(47)~~ contribution is

~~Because the Newton emissivity uncertainty is explicitly controlled by the Jacobian of the inversion, this term remains structurally bounded whenever emissivity is observable. As irradiance contrast weakens, the Jacobian decreases smoothly, leading to controlled and physically interpretable increase in emissivity-driven temperature uncertainty rather than the non-physical divergence associated with the linearized emissivity . Correlated irradiance errors therefore do not destabilize the temperature retrieval; instead, uncertainty growth remains governed by emissivity observability and inversion conditioning.~~

$$\sigma_{T_s,\epsilon} = \left|\frac{\partial T_s}{\partial \epsilon}\right| \sigma_{\epsilon,corr}. \tag{41}$$

The ~~total correlated-error surface temperature uncertainty is obtained by combing the~~ correlated irradiance-driven ~~and emissivity-driven contributions:~~

~~(48)~~ contribution follows from

~~This expression represents the physically realistic uncertainty of the corrected surface temperature in the presence of shared calibration effects, atmospheric coherence, and cross-channel coupling. In well-conditioned cases, the total uncertainty is dominated by the irradiance-driven component and closely resembles the independent-error baseline. In weakly conditioned cases, emissivity-driven uncertainty becomes dominant but remains bounded and diagnostically interpretable due to Jacobian control.~~

$$\sigma_{T_s,L} = \left|\frac{L_1^{-3/4}+L_2^{-3/4}}{8\sigma^{1/4}}\right| \sigma_L \sqrt{(1\ 1)\begin{pmatrix}1 & \rho_L\\ \rho_L & 1\end{pmatrix}\begin{pmatrix}1\\1\end{pmatrix}}, \tag{42}$$

~~The correlated-error decomposition demonstrates that the bounded uncertainty behavior observed in the Newton-based surface temperature retrieval is not an artifact of the independent-error assumption. Instead, it reflects the intrinsic conditioning of the inversion and the explicit control of~~ Combining the irradiance- and emissivity-driven ~~amplification.By incorporating physically realistic covariance, the correlated formulation provides a robust and interpretable uncertainty estimate and confirms that adaptive temporal pairing improves temperature stability primarily by strengthening emissivity observability rather than by suppressing measurement noise.~~

~~3.6 Algorithmic integration and flow~~

~~The integration of the irradiance modeling, adaptive data selection and nonlinear inversion described in the preceding sections is summarized in the diagnostics framework show in Figure 1. This flowchart illustrates the logical progression from the initial selection of high-frequency temporal pairs to the final retrieval of the corrected surface temperature and uncertainty decomposition.~~ terms gives the total propagated temperature uncertainty

~~As shown in Figure 1, the retrieval is fundamentally governed by the Quasi-Steady Condition (Step), which serves as a physical and numerical filter. By enforcing a constraint on the change in apparent surface temperature between observation times (), the algorithm adaptively adjusts the temporal separation to maximize irradiance contrast while preserving the physical assumption of emissivity invariance.~~

$$\sigma_{T_s,corr} = \sqrt{\sigma^2_{T_s,L} + \sigma^2_{T_s,\epsilon}}. \tag{43}$$

~~The transition from a linearized diagnostic estimate (Step 4) to the full Newton inversion (Step 5) ensures that the retrieval handles the nonlinear emissivity-temperature coupling rigorously. Furthermore, the framework incorporates post-hoc diagnostics and uncertainty decomposition (Steps 6 and 8), ensuring that every retrieved temperature is supported by an explicit assessment of inversion conditioning and parameter observability. This integrated approach allows the framework to remain structurally extensible to more complex radiative transfer scenarios while maintaining the diagnostic transparency required for high-precision ground-based validation~~ These quantities are propagated retrieval uncertainties and are not assumed to be calibrated confidence intervals; empirical coverage is evaluated separately using the known-truth experiment. The interpretation of local sensitivity and uncertainty follows standard inverse-problem reasoning (Tarantola, 2005; Menke, 2012; Aster et al., 2019).

4 Experimental setup and validation framework

~~**Figure 1.** Flowchart of the diagnostic-driven retrieval framework for broadband land surface temperature () and surface emissivity~~ (Two complementary validation strategies are used (Fig. 2). The ~~process integrates adaptive temporal pairing () constrained by the quasi-steady apparent surface temperature condition () , followed by a nonlinear Newton-Raphson inversion with explicit convergence diagnostics. The framework concludes with formal uncertainty propagation and decomposition into irradiance-driven and emissivity-driven components to assess retrieval reliability prior to in-situ performance evaluation.~~ field experiment uses ground-based longwave observations from nine SURFRAD and BSRN stations spanning vegetated, mixed, and bare/desert environments. The second is a physics-based known-truth experiment in which emissivity and surface temperature are prescribed independently of the retrieval and broadband longwave observations are generated from exact forward physics. Both validation arms are processed with the same pre-specified conditioning-controlled retrieval formulation.

~~4 Experimental setup and validation framework~~

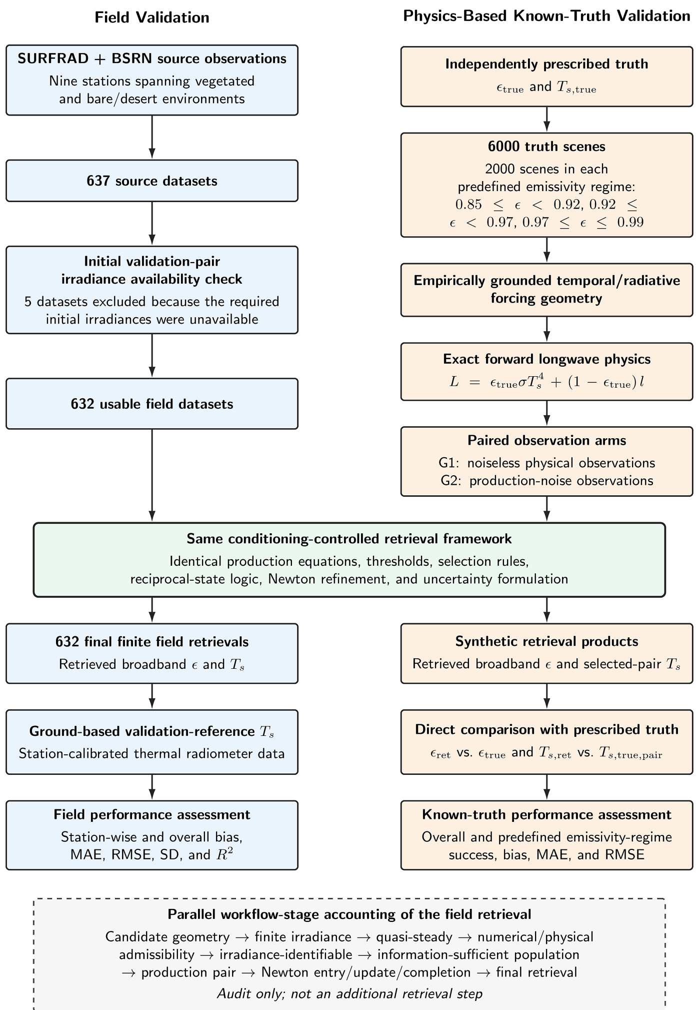

Figure 2. Field and physics-based known-truth validation architecture. The field arm retains 632 usable datasets from 637 source datasets; the synthetic arm contains 6000 prescribed truth scenes evaluated as noiseless (G1) and production-noise (G2) observations. Both arms use the same conditioning-controlled retrieval framework.

~~This section describes the observational datasets, reference products, and contextual background used to evaluate the proposed broadband emissivity and surface temperature retrieval . It establishes the scope of the analysis, the basis for independent validation, and the limitations of commonly used approaches, thereby providing the necessary frameworkfor interpreting the results presented in Sect. 5.~~

4.1 ~~Data coverage and representativeness~~Ground-based field-validation dataset

The ~~Surface Radiation Budget Network (SURFRAD) provides long-term, quality-controlled broadband irradiance measurements (Augustine et al., 2005). Four stations-Bondville (Illinois~~field population combines observations from seven SURFRAD stations and two BSRN stations: Bondville (BON), Desert Rock (DRA), Fort Peck (~~Montana~~FPK), Goodwin Creek (~~Mississippi), and~~GWN), Penn State (PSU), Sioux Falls (~~South Dakota)were used in this study. These stations operate in climatologically diverse regions and span a range of land cover types, surface conditions, and atmospheric regimes, including agricultural landscapes, grasslands, and mixed natural surfaces. As such, they provide a representative testbed for evaluating broadband emissivity observability and surface temperature retrieval under varying environmental conditions.~~ SXF), Table Mountain (TBL), Cabauw (CAB), and Gobabeb

Table 1. Validation datasets and station composition. The initial-irradiance exclusion refers only to the prescribed validation-pair availability check.

Network	Station	Code	Source datasets	Excluded at initial irradiance check	Final retrievals	Retention (%)
SURFRAD	Bondville	BON	70	1	69	98.57
BSRN	Cabauw	CAB	48	1	47	97.92
SURFRAD	Desert Rock	DRA	50	0	50	100.00
SURFRAD	Fort Peck	FPK	75	0	75	100.00
BSRN	Gobabeb	GOB	194	3	191	98.45
SURFRAD	Goodwin Creek	GWN	50	0	50	100.00
SURFRAD	Penn State	PSU	26	0	26	100.00
SURFRAD	Sioux Falls	SXF	40	0	40	100.00
SURFRAD	Table Mountain	TBL	84	0	84	100.00
TOTAL	**All stations**	**ALL**	**637**	**5**	**632**	**99.22**

A total of 637 source datasets entered the workflow audit. Five datasets (one BON case, one CAB case, and three GOB cases) did not contain the required finite initial irradiances and were excluded, leaving 632 usable field datasets. All 632 usable cases produced final finite production retrievals.

~~both well-conditioned and weakly conditioned scenarios. All diagnostic, emissivity estimates (linearized and Newton-based), and corrected surface temperatures reported in subsequent sections are derived exclusively from this multi-site, multi-season dataset~~637 source datasets entered the workflow audit. Five datasets (one BON case, one CAB case, and three GOB cases) did not contain the required finite initial irradiances and were excluded, leaving 632 usable field datasets. All 632 usable cases produced final finite production retrievals.

4.2 ~~Reference emissivity and surface temperature for~~ Ground-based surface-temperature validation reference

The ~~Surface Radiation Budget Network Independent reference values were required to evaluate the retrieved surface temperatures. For this purpose, broadband surface emissivity at each SURFRAD site was derived from satellite-based emissivity products. Specifically, emissivities from MODIS thermal infrared bands 31 and 32 were obtained from the 8-day MODIS land surface temperature product for dates nearest to the SURFRAD observations .~~

~~The narrowband emissivities were converted to broadband emissivityusing the method proposed by (Wang et al., 2005; Wan, 2014). These broadband emissivities were then combined with SURFRAD upwelling longwave irradiance measurementsand the Stefan-Boltzmann law to compute reference land surface temperatures. The resulting temperatures serve as external benchmark for evaluating the performance of the proposed retrieval algorithm. It is emphasized that satellite-derived emissivities and temperatures are used solely for validation purposes and are not used as inputs to the emissivity or surface temperature retrievalalgorithm developed in this study.~~ field comparison uses a ground-based validation-reference temperature $T_{s,ref}$. It is derived from station-calibrated ground-based longwave thermal-radiometer observations combined with externally specified broadband emissivity,

~~4.3 Context within existing SURFRAD-based approaches~~

$$T_{s,ref} = \left(\frac{L_{ref} - \left(1 - \epsilon_{ref}\right) l_{ref}}{\epsilon_{ref} \sigma} \right)^{1/4} . \qquad (44)$$

~~Previous studies attempting to derive land surface temperaturesfrom SURFRAD longwave irradiance measurements have often relied on satellite-derived narrowband emissivities, typically from MODIS thermal infrared bands (e. g., bands 29, 31, and 32). In many cases, emissivity values are obtained from global products such as MYD11C3, which provide monthly averages at a coarse spatial resolution (approximately 5 km).~~ The field reference and retrieval are therefore not statistically independent in their irradiance measurements: both ultimately involve ground-observed longwave irradiance. The distinction is that ϵ_{ref} is externally specified and is not supplied to the proposed emissivity retrieval. The field arm consequently validates combined emissivity-temperature retrieval behaviour under real observations rather than providing independent broadband-emissivity truth.

~~Common practice involves selecting emissivity values from pixels nearest to the SURFRAD site location, applying quality masks, and averaging over a small spatial~~

~~window (e.g.,~~ For the SURFRAD reference records, externally supplied broadband emissivity information was used to derive the validation-reference temperatures. For Cabauw and Gobabeb, the validation-reference temperature was constructed from the nearest 1-min upwelling and downwelling longwave observations at the Landsat acquisition time together with the corresponding Landsat-8 3 ~~x~~ $\times$ 3 ~~) pixels. While widely used , this approach introduces several sources of uncertainty, including: spatialmismatch between point-scale radiometric measurements and coarse satellite pixels; temporalmismatch between instantaneous in situ observations and multi-day or monthly satellite composites; spectral mismatch between narrowband satellite emissivities and broadband longwave irradiance exchange. The combined effect of these mismatches can significantly degrade the reliability of surface temperatures estimates derived from SURFARD irradiance measurements.~~

~~5 Results and discussion~~

~~This section presents a comprehensive evaluation of the proposed broadband emissivity and surface temperature retrieval algorithm, with emphasis placed on numerical and physical consistency rather than accuracy alone. Results are first examined in terms of Newton convergence characteristics, conditioning, and diagnostic indicators that govern the stability of the nonlinear inversion. The performance of the retrieved surface emissivity is then assessed, followed by validation of the corrected surface temperature against independent in-situ measurements. Finally, a detailed uncertainty analysis is presented, including explicit decomposition of surface temperature uncertainty into emissivity-driven and irradiance-driven components. Together, these results demonstrate that the reliability of the retrieval is governed by its numerical conditioning and diagnostic behavior, providing a transparent basis for interpreting accuracy and uncertainty across observational conditions.~~

~~5.1 Newton convergence behaviour and conditioning~~

~~The numerical stability and conditioning of the nonlinear emissivity inversion were first evaluated through a set of Newton convergence diagnostics derived directly from the iterative solution process. These diagnostics are independent of retrieval accuracy and instead assess whether the inversion is physically observable and numerically well posed under available radiometric constraints.~~

~~Figure 2 illustrates that residuals remain small across the full range of Jacobian values, confirming irradianceconsistency. Importantly, no cases exhibit vanishing or near-singular Jacobians, indicating that the inversion avoids flat or ill-conditioned regimes. This behaviour confirms that the adaptive temporal pairing strategy successfully selects irradiance pairs that preserve physical observability while maintaining numericalstability.~~

~~**Figure 2.** Relationship between the final Newton residual magnitude and the minimum absolute Jacobian valueencountered during inversion. The absence of large residuals at small Jacobian magnitudes indicates that the emissivity inversion remains well conditioned and avoids singular or non-singular behavior across all cases.~~ mean emissivity.

~~The observed order of convergence, computed from successive Newton iterates, is~~

~~summarized in Figure 3 and reported quantitatively in Table 1. The distribution ofvalues is strongly concentrated near unity, with several cases marginally exceeding 0.9998 before rounding. When rounded to four decimal places, these values cluster tightly around one. While classical Newton theory predicts quadratic convergence in~~ The externally specified emissivities used only to construct the field temperature reference are themselves subject to spectral, spatial, temporal, and representativeness uncertainty. The field comparison is therefore interpreted as a realistic benchmark of the combined emissivity–temperature retrieval rather than as independent emissivity truth; direct broadband-emissivity accuracy is evaluated only in the ~~asymptotic neighbourhood of an exact root, near-linear convergence is expected in the present application for several reasons: the inversion involves fractional-power irradiance terms,measurement noise is present in both upwelling and downwelling irradiances, and a fixed number of iterations is employed rather than asymptotic convergence to machine precision. Under these conditions,the observed convergence behaviour is stable, predictable,and fully consistent with theoretical expectations.~~ prescribed-truth experiment.

4.3 Field performance metrics and workflow accounting

~~**Figure 3.** Distribution of the observed Newton convergence order, rounded to four decimal places. Values cluster tightly around unity,with several cases approaching near-quadratic convergence before rounding, indicating stable and predictable nonlinear behavior under the fixed-iteration Newton scheme.~~ For each field retrieval, the signed temperature error is $e_{T,i} = T^{ret}_{s,i} - T^{ref}_{s,i}$. Performance is summarized by bias, MAE, RMSE, standard deviation of signed error, and squared Pearson correlation coefficient R^2. A separate read-only audit tracks candidate geometry, finite irradiance, quasi-steady screening, numerical/physical admissibility, irradiance identifiability, information sufficiency, production-pair selection, Newton progression, and final retrieval. The audit does not impose additional rejection criteria and does not modify the production retrieval. Detailed scene- and pair-level accounting is given in Appendix A.

~~Crucially, no cases exhibit sub-linear convergence or erratic behavior, indicating that the Newton updatesremain well directed throughout the inversion. The absence of convergence degradation further supports the conclusion that the emissivity inversion remains well conditioned across the full dataset. The numerical complexity of the retrieval involves two distinct iteration processes. The Newton-Raphson solver loop was executed with a fixed maximum count, to allow for comprehensive diagnostic analysis. The adaptive temporal adjustment loop measures the effort required to select a numerically stable data pair. The count reported in Table 1 (labeled)and shown in Figure 4 quantifies this adaptive effort. For the vast majority of cases, is low, indicating that the initial temporal constraints already provided strong irradiance contrast. This distinction is critical: confirms data suitability while the analysis of the fixedconfirms solver stability. Because the observed convergence orderremains high (near 1.0) and stable (Figure 3), the fixed countis demonstrated to be sufficient to achieve a solution precision constrained by~~ Across the 632 usable field scenes, the ~~inherent irradiance uncertainty~~audit contains 88,154 geometry-valid candidate pairs, of which 88,135 have finite irradiances, 81,682 satisfy the quasi-steady and denominator-validity stages, 68,525 retain a physically admissible linear-emissivity state, and 63,190 satisfy the irradiance-identifiability condition. At scene level, all

632 usable datasets contain at least one admissible and identifiable pair, all 632 enter Newton–Raphson refinement, and all 632 complete eight valid Newton updates. Appendix A provides the corresponding station-wise and stage-by-stage accounting.

~~**Table 1.** Summary of the number of adaptive adjustments, minimum Jacobian magnitude, residual magnitude, and observed order of convergence for each dataset. These diagnostics quantify emissivity observability, numerical conditioning, and convergence behavior of the inversion and are used to distinguish well-conditioned and weakly conditioned retrievals.~~

4.4 Physics-based known-truth synthetic validation

The synthetic validation contains $N_{syn} = 6000$ independent truth scenes. A fixed random seed, rng(858), is used for reproducibility. Exactly 2000 scenes are generated in each of three emissivity regimes: $0.85 \le \epsilon_{true} < 0.92$, $0.92 \le \epsilon_{true} < 0.97$, and $0.97 \le \epsilon_{true} \le 0.99$. The initial true surface temperature is prescribed independently over 270-330 K. Synthetic temporal forcing is empirically grounded by bootstrap sampling observable temporal-driver states derived from the 632 field cases.

For each time sample, the true surface emission is $S(t) = \sigma T_s^{true}(t)^4$, and exact upwelling irradiance is generated as

~~Figure 5 illustrates the relationship between the selected temporal separation and the retrieved Newton emissivity. The absence of any systematic dependence confirms that adaptive temporal pairing does not influence the emissivity solution itself, but instead functions as a neutral conditioning mechanism. This behavior is essential, as it demonstrates that convergence is achieved through appropriate data selection rather than through implicit modification of the inversion physics. The quasi-steady apparent surface temperature constraint therefore plays a critical dual role. Physically, it preserves the assumption that emissivity remains invariant over the selected time interval. Numerically, it prevents ill-posed inversions in which irradiance differences are dominated by surface temperature variability rather than emissivity sensitivity. Without this constraint, increasing temporal separation would introduce emissivity-temperature coupling that flattens the inversion surface and inflates uncertainty.~~

$$L(t) = \epsilon_{true} S(t) + (1 - \epsilon_{true})\, l(t). \tag{45}$$

~~Convergence is therefore achieved through informed data selection rather than modification of the underlying physics. Consistent with the convergence diagnosis above, the results shown in Figure 5 demonstrate that this approach improves numerical conditioning while preserving physical neutrality, enabling stable emissivity retrieval across diverse surface and atmospheric conditions and providing a robust foundation for subsequent uncertainty analysis and surface temperature results.~~ Thus, ϵ_{true} enters only through the forward model and is never derived from, fitted to, or conditioned on the retrieval result.

4.5 Noiseless and production-noise synthetic experiments

~~**Figure 4.** Distribution of adaptive dt-pair iteration counts required to obtain a physically admissible initial emissivity estimate. The low iteration counts observed for nearly all cases indicate that only minimal temporal adjustment is needed to satisfy the quasi-steady surface temperature constraint, confirming strong temporal observability~~Each truth scene is used for two paired experiments. G1 contains the exact physically generated longwave observations with no additional measurement perturbation and therefore isolates retrieval/inversion behaviour. G2 uses the same 6000 truth scenes but adds a correlated production-noise realization drawn from the covariance structure defined in Eq. (16) before unchanged Savitzky-Golay processing. Apart from this perturbation, G1 and G2 use identical truth states and the same retrieval implementation.

~~Taken together, the residual magnitude, Jacobian strength, observed convergence order, and adaptive iteration counts provide complementary evidence that the Newton emissivity inversion is numerically stable, well-conditioned, and converges in a physically meaningful manner across diverse surface and atmospheric conditions. These diagnostics demonstrate that convergence arises from genuine irradiance information content rather than numerical artifact, establishing a robust foundation for interpreting the emissivity and surface temperature retrieval results presented in subsequent sections.~~ All 6000 generated scenes remain in the denominator used to compute retrieval success:

$$f_{success} = \frac{N_{successful}}{6000}. \tag{46}$$

~~**Figure 5.** Relationship between the selected time separationand the retrieved Newton emissivity. The adaptive dt-pair selection adjusts temporal spacing only as needed to maintain quasi-steady apparent surface temperature, improving numerical conditioning without altering the underlying irradiance model~~Bias, MAE, and RMSE require a finite retrieved value and are therefore calculated over successful retrievals only. For T_s, error is evaluated against the true temperature corresponding to the selected production pair.

~~5.2 Emissivity retrieval results~~

~~This section evaluates the broadband emissivity retrieval performance, emphasizing the critical distinction between numerical magnitude and retrieval stability. Figure 6 compares the emissivity values obtained from the Newton inversion against those derived from the linearized approximation. While both approaches yield estimates of comparable magnitude, indicating that the linearized formulation provides a mathematically consistent starting point, this numerical agreement masks fundamental differences in the quality and robustness of the solutions.~~

5 Results and discussion

~~The primary finding is that the reliability of the retrieved emissivity is not governed by its value, but by the conditioning of the framework used to find it. As establishedin~~

~~the sensitivity analysis (Sect. 3.4.1), the linearized estimate is a first-order diagnostic that is highly susceptible to extreme uncertainty amplification under weak temporal contrast. In contrast, the Newton-based solution maintains its physical integrity across the entire dataset. The stability of the Newton inversion, enabled y explicit Jacobian control, ensures that the retrieval remains bounded even in low signal-to-noise ratio environments where the linearized model begins to exhibit non-physical behavior. Consequently, while the linearized estimate is retained as an efficient initialization tool,~~ The results follow the physical and numerical sequence through which retrieval reliability is established. Temporal-pair selection and stability are examined first, followed by reciprocal-state applicability, Newton behaviour, the ~~Newton-based solution is identified as the only physically meaningful estimate capable of supporting high-precision surface temperature retrievals.~~

~~**Figure 6.** Comparison of emissivity obtained from the Newton inversion and the linearized approximation. While both approaches yield similar emissivity values, the linearized estimate is retained only as a diagnostic due to its strong conditioning dependence~~

~~The contrasting uncertainty behavior of the two formulations is illustrated in Figure 7, which compares correlated emissivity uncertainty for the Newton-retrieved emissivity (to panel) and the linearized emissivity (bottom panel). Although the retrieved emissivity values are similar, the associated uncertainty differs markedly. The linearized emissivity uncertainty is substantially larger and more variable, requiring a separate scale for visualization. This behavior reflects the strong conditioning dependence inherent in the linearized formulation, where uncertainty amplification is dominated by weak temporal irradiance contrast and denominator sensitivity. In contrast, the Newton emissivity uncertainty remains bounded and smoothly varying across all cases, consistent with Jacobian-controlled uncertainty propagation. This result confirms thatthe Newton inversion suppresses non-physical amplification by explicitly accounting for emissivity-temperature coupling and local curvature of the irradiance balance equation.~~

contrast-sensitivity-uncertainty relationship, field emissivity behaviour, field surface-temperature validation, and physics-based known-truth validation.

~~**Figure 7.** Comparison of correlated emissivity uncertainty components: Newton-retrieved emissivity uncertainty, (top), and linearized emissivity uncertainty (bottom), shown on separate scales. Although the retrieved emissivties are comparable, linearized is markedly larger and more variable, reflecting the stronger sensitivity of the linearized formulation to irradiance-based conditioning~~

5.1 Temporal-pair selection and stability

Figure 3 characterizes the progressive selector over the complete 632-case field population. Of the 632 retrievals, 628 were selected through the stable-centre pathway and only four required fallback selection. The median selected production-pair separation was 3.0 min. These results show that, for the overwhelming majority of cases, the progressive search identified a locally stable emissivity population without exhausting the prescribed fallback pathway.

~~Figure 8 further examines emissivity uncertainty under independent and correlated irradiance error assumptions. Panel~~

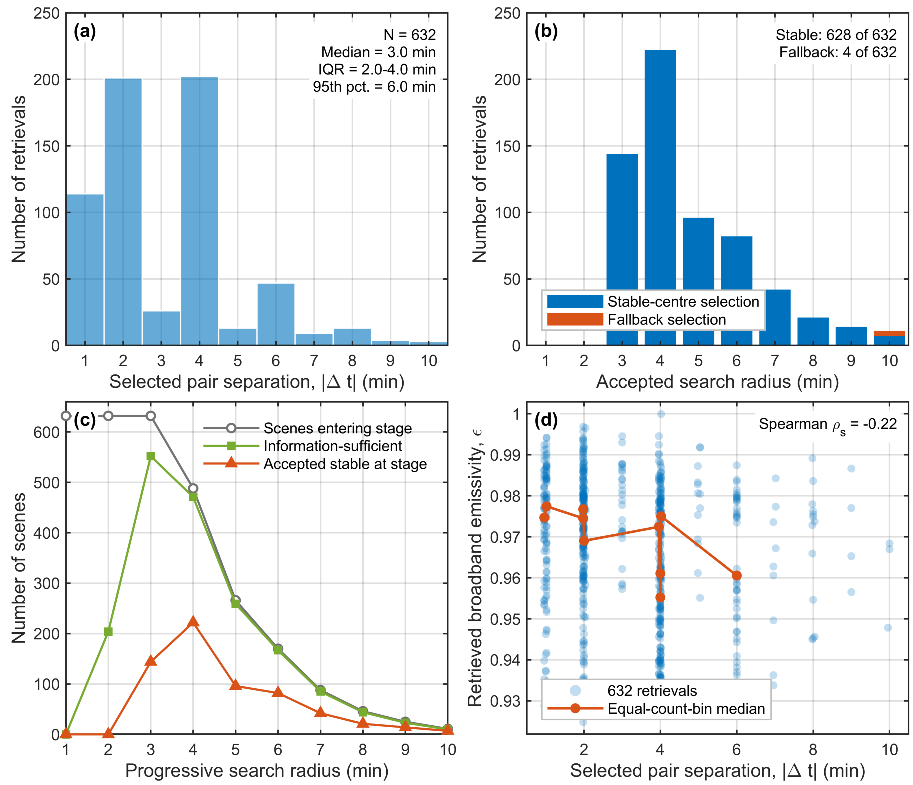

Figure 3. Temporal-pair selection and progressive information sufficiency for the 632 field retrievals. (a) Selected production-pair separation. (b) Accepted search radius, distinguishing stable-centre and fallback pathways. (c) Progressive growth of information-sufficient and stable-stage populations with search radius. (d) Selected pair separation versus retrieved emissivity.

(a) ~~shows Newton emissivity uncertainty assuming independent and correlated irradiance errors; when irradiance covariance is accounted for, the correlated-error formulation produces consistently larger uncertainty estimates. Panel~~ Selected production-pair separation. (b) ~~presents the same uncertainties on a case-by-case basis, revealing that correlation primarily introduces a consistent offset rather than altering the relative structure of uncertainty across cases. This behavior indicates that while irradiance covariance affects the absolute scale of emissivity uncertainty, it does not fundamentally change which cases are well or weakly conditioned. The persistence of bounded uncertainty under correlated errors confirms the stability of the Newton retrieval is not an artifact of idealized noise assumptions, but a consequence of improved emissivity observability.~~

~~**Figure 8.** (a) Newton emissivity uncertainty under independent and correlated irradiance errors, with correlation increasing uncertainty magnitude; (b) corresponding case-wise uncertainties showing similar structure but systemic offset due to irradiance covariance.~~

~~Table 2 summarizes the broadband emissivity retrieval results and associated~~

~~uncertainty estimates under both independent and correlated error assumptions. Newton and linearized emissivityvalues are reported alongside their corresponding uncertainty estimates, enabling direct comparison of retrieval magnitude and uncertainty behaviour. The table reinforces the graphical results: while emissivity values are broadly consistent between methods, the Newton-based uncertainty remains controlled under both error assumptions, whereas the linearized uncertainty exhibits strong sensitivity to conditioning. Together, these results demonstrate that reliable broadband emissivity retrieval can be achieved without externally prescribed emissivity products when numerical conditioning, convergence diagnostics, and uncertainty propagation are treated as integral components of the retrieval framework.~~

~~**Table 2.** Broadband emissivity retrieval results and associated uncertainty estimates under independent and correlated error assumptions, showing Newton and linearized emissivity values together with emissivity uncertainties propagated from broadband longwave irradiance measurements.~~

~~5.2.1 Analysis of emissivity observability and inversion conditioning~~

~~The fundamental reliability of the broadband emissivity retrieval is governed by the interplay between the physical irradiance environment and the numerical stability of the Newton inversion. Figure 9 deconstructs this relationship by examining emissivity uncertainty and Jacobian conditioning as a function of irradiance contrast. Panel (a) illustrates the absolute uncertainty of the Newton-retrieved emissivity () across a spectrum of irradiance contrast conditions. A distinct power-law relationship is observed: as irradiance contrast approaches zero, representing a collapse of the signal-to-noise ratio where surface and atmospheric irradiances become nearly identical, the emissivity uncertainty increases from a baseline of approximately 0.006 to peak values exceeding 0.016. This trend aligns with theoretical expectations regarding the physical limit of emissivity observability ; as the irradiance difference that labels the surface emissivity vanishes, the parameter becomes inherently more difficult to constrain~~Accepted search radius, distinguishing stable-centre and fallback pathways. (c) Progressive growth of information-sufficient and stable-stage populations with search radius. (d) Selected pair separation versus retrieved emissivity.

~~This physical degradation is directly explained by the numerical conditioning shown in Panel (b). The minimum Jacobian magnitude (), which represents the sensitivity of the irradiance balance to changes in emissivity, exhibits a strong positive correlation with irradiance contrast. Jacobian values rise from near 150 at low contrast to approximately 400 in high-contrast regimes. Mathematically, the Jacobian defines the numerical grip the Newton solver has on the solution space; the lower Jacobian magnitudes observed at low contrast confirm that the inversion surface becomes locally flatter, thereby amplifying the propagation of measurement noise into the~~

The relationship in Fig. 3d is used as an empirical check for systematic displacement of the emissivity ~~estimate. These observations confirm that the difficulty in retrieving emissivity at low contrast is not failure of the algorithm, but a fundamental property of the irradiance physics and inversion conditioning~~solution with increasing pair separation. Within the retained population, no strong monotonic shift is evident. Quasi-steady screening is therefore interpreted as one component of the selection chain rather than a complete observability test; stable production selection also requires irradiance identifiability and sufficient independent information.

5.2 Physical-state applicability of the reciprocal emissivity formulations

~~**Figure 9.** Determinants of the emissivity retrieval observability and conditioning~~Following selected-pair thermal correction, the retrieval evaluates whether the surrounding radiative state supports one of the exact reciprocal emissivity transformations. Figure 4 presents the two physical configurations for which the applicability boundaries have a direct radiative interpretation.

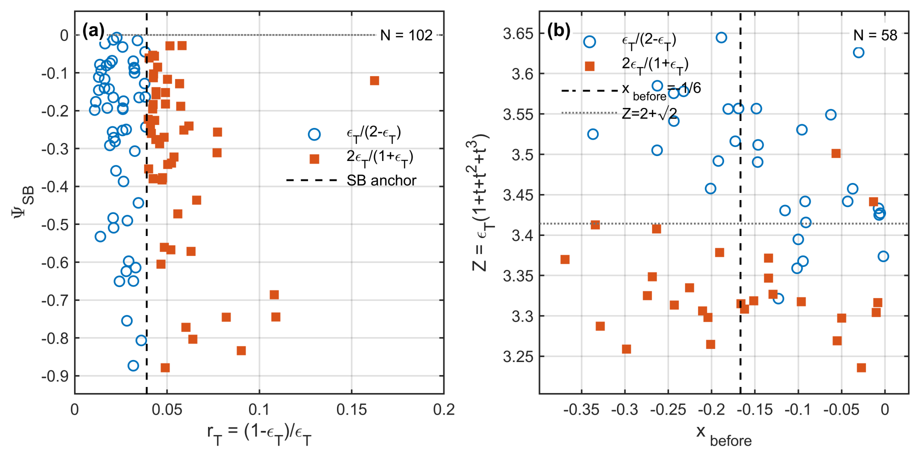

Figure 4. Physical-state applicability of the reciprocal emissivity formulations. (a) Stefan-Boltzmann-controlled configuration expressed in the physical-state space. (b) Reciprocal-conductance configuration expressed in the corresponding physical-state space. The plotted boundaries are the pre-specified physical applicability conditions used by the production selector.

. (a) ~~Newton-based emissivity uncertainty () as a function of irradiance contrast; (b) minimum Jacobian magnitude (), illustrating the numerical strength of the inversion; and (c) the fractional contribution of emissivity to the total uncertainty budget. These panels illustrate that while low irradiance contrast degrades the Mathematical conditioning (Panel b) and increase parameter uncertainty (Panel a), the Newton framework prevents the instability from dominating the final temperature product (Panel c).~~ Stefan-Boltzmann-controlled configuration expressed in the - state space. (b) Reciprocal-conductance configuration expressed in the - state space. The plotted boundaries are the pre-specified physical applicability conditions used by the production selector.

~~A critical finding of this analysis is the robustness of the temperature-emissivity coupling control, as is evidenced in Panel (c). Despite the three-fold increase in emissivity uncertainty and the significant weakening of the Jacobian at low contrast, the fraction of total temperature uncertainty due to emissivity remains remarkably stable at approximately 34%. This indicates that while emissivity itself becomes harder to retrieve under poor irradiance conditions, the Newton-based formulation~~

~~successfully bounds its propagation into the final temperature product. The primary implication of these results is that the retrieval framework is diagnostically self-regulating. By explicitly accounting for the Jacobian strength, the method ensures the emissivity driven errors do not catastrophically amplify, allowing for reliable surface temperature estimation even when the signal-to-noise ratio for emissivity is significantly challenged. This diagnostic transparency ensures that the resulting precision is formally supported by the internal physics of the inversion rather than by external assumptions.~~ The Stefan-Boltzmann-controlled configuration occurs in 102 of the 632 field cases, while 58 cases occupy the reciprocal-conductance configuration. The remaining 472 cases exhibit other production-state signatures and are not represented in these two diagnostic panels. The reciprocal transformation is therefore state dependent rather than universally applied, and the branch choice is made before comparison with the field validation reference.

~~5.3 Surface temperature uncertainty analysis~~

5.3 Newton numerical behaviour within the retained population

~~To provide a rigorous evaluation of the Newton-based retrieval, the following sections deconstruct the surface temperature uncertainty () into its fundamental physical and numerical drivers. This analysis moves beyond aggregate error metrics to examine the stability of the inversion under diverse conditions. Specifically, Sect. 5.3.1 investigates how the uncertainty budget responds to physical scene dynamics, focusing on the critical role of irradiance contrast and its impact on the signal-to-noise ratio. Subsequently, Sect. 5.3.2 evaluates the structural stability of the retrieval across discrete cases, quantifying how the transition from the idealized independent noise to realistic correlated error assumptions scales the absolute uncertainty without compromising the underlying sensitivity of the framework~~Figure 5 evaluates Newton-Raphson behaviour after candidate screening, production-pair selection, and physical-state conditioning. Figure 5a relates the final absolute residual to the minimum local emissivity sensitivity, while Fig. 5b shows the distribution of that sensitivity across the retained field population.

~~5.3.1 Irradiance contrast and SNR dynamics~~

~~The relationship between retrieval reliability and the physical state of the scene is best characterized by examining the dependence of surface temperature uncertainty () on irradiance contrast. As shown in the scatter analysis of Figure 10, the Newton-based formulation exhibits a clear, physically consistent response to varying atmospheric and surface conditions. This relationship is essentially a function of the signal-to-noise ratio (SNR) inherent in the irradiance environment.~~

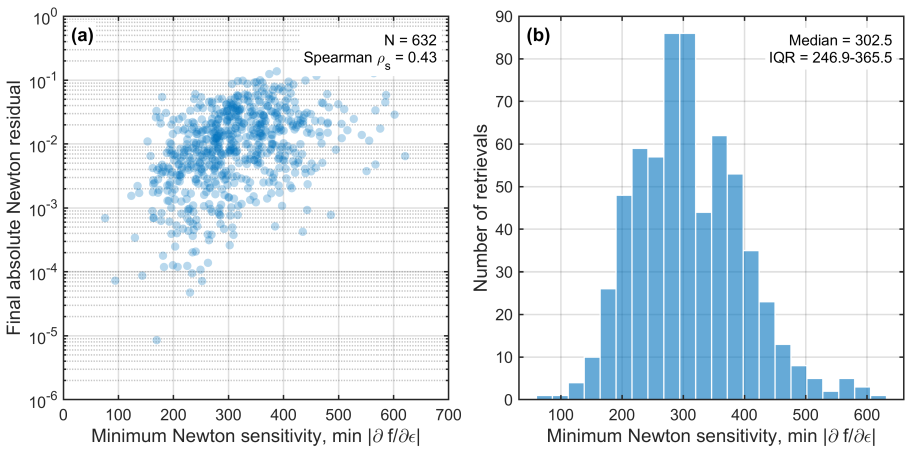

Figure 5. Newton numerical behaviour within the retained 632-case field population. (a) Final absolute nonlinear residual versus minimum absolute emissivity sensitivity encountered during the fixed eight-update trajectory. (b) Distribution of the minimum absolute sensitivity.

~~Panels (a) and~~ (b) ~~demonstrate that as irradiance contrast approaches zero, representing a regime where the signal-to-noise ratio is severely degraded because the surface and atmospheric signals become increasingly indistinguishable, and the absolute uncertainty in surface temperature increases. Crucially, this increase is not catastrophic; rather than exhibiting the numerical instability common in poorly conditioned inversions under low SNR conditions, the uncertainty remains bounded and diagnostically interpretable. This indicates that the Newton-based successfully preserves the inversion's physical meaning even when the observational signal is weak~~Distribution of the minimum absolute sensitivity.

The ~~fractional decomposition provided in Panel (c) reveals a fundamental characteristic of the uncertainty budget in relation to this signal-to-noise ratio. Irradiance-driven uncertainty consistently dominates the budget, accounting for approximately 65% to 67% of the total correlated error. This suggests that the primary limit on retrieval precision is the inherent measurement noise and its propagation through the Planck function, which sets the baseline for the signal-to-noise ratio.~~

~~Interestingly as irradiance contrast increases, effectively improving the signal-to-noise ratio, the irradiance driven fraction exhibits a marginal decline~~figure characterizes the numerical state of accepted production retrievals and should not be interpreted as evidence that arbitrary temporal pairs are well conditioned. Weakly identifiable and numerically inadmissible candidates are addressed earlier in the workflow. Small residuals establish consistency with the nonlinear equation at the retrieved state, while the ~~emissivity-driven fraction shows a corresponding slight increase. This shift suggests that as the irradiance noise becomes a relatively less obstructive part of the signal, the accurate characterization of surface emissivity becomes a progressively more significant factor in achieving a high-precision temperature retrievals. In high SNR environments, the limiting factor shifts slightly from raw measurement noise toward the physical constraints of emissivity modeling~~derivative magnitude quantifies local sensitivity; neither quantity alone is treated as a complete observability criterion.

5.4 Radiative contrast, inversion sensitivity, and propagated uncertainty

~~**Figure 10.** Surface temperature uncertainty components plotted as a function of irradiance contrast. Panel (a) shows the irradiance-driven and emissivity-driven surface temperature uncertaintyunder independent error assumptions; panel (b) shows the corresponding components under correlated irradiance error assumptions; panel (c) shows the fractional contribution of the irradiance-driven and emissivity-driven components to the total surface temperature uncertainty for the correlated case. Across all panels, uncertainty structure follows the same irradiance sensitivity patterns, while correlation primarily scales the uncertainty magnitude without altering the relative contribution of the two pathways~~Figure 6 links the selected-pair upwelling contrast $|\Delta L|$ to local nonlinear sensitivity and propagated uncertainty. Across the 632 retrievals, the Spearman correlation between $|\Delta L|$ and correlated emissivity uncertainty is -0.4026, while the correlation between $|\Delta L|$ and minimum sensitivity is $+0.4026$. Minimum sensitivity and correlated emissivity uncertainty have a rank correlation of -1.0000.

~~5.3.2 Case-level stability and correlation scaling effects~~

~~While the previous analysis establishes how signal-to-noise ratio influences the error budget, Figure 11 examines the case-by-case structural stability of the uncertaintycomponents across 39 discrete retrieval scenarios. This perspective allows for a direct comparison between idealized (independent) and realistic (correlated) irradiance errors assumptions.~~

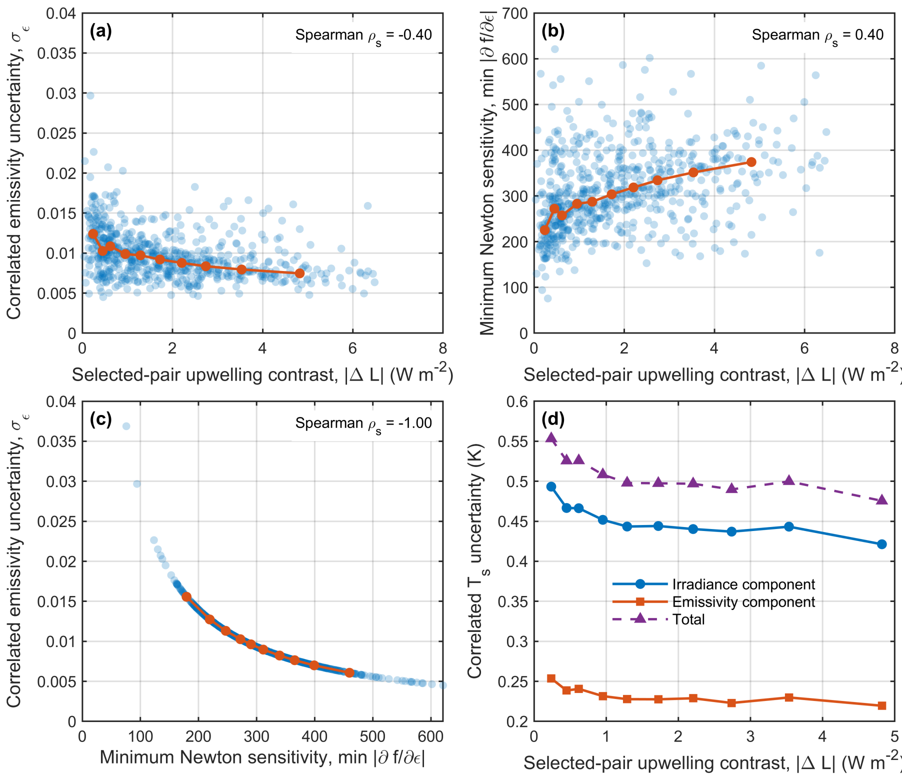

Figure 6. Conditioning and propagated uncertainty. (a) Selected-pair upwelling contrast $|DeltaL|$ versus correlated emissivity uncertainty. (b) $|DeltaL|$ versus minimum nonlinear emissivity sensitivity. (c) Minimum sensitivity versus correlated emissivity uncertainty. (d) Irradiance-driven, emissivity-driven, and total correlated T_s uncertainty components.

~~Under both assumptions, the total surface temperature uncertainty() and its constituents, irradiance-driven () and emissivity-driven () components track one another with high structural fidelity. The peaks and valleys in the uncertainty profile occur at identical case indices across both panels, confirming that the underlying sensitivity is governed by the same Jacobian structure and irradiance sensitivities regardless of whether the error is modeled as independent or correlated~~ .

~~**Figure 11.** Decomposition of total corrected surface temperature uncertaintyinto irradiance-driven and emissivity-driven components for correlated (top) and independent (bottom) error assumptions. All components share similar structure because they depend on the same irradiance sensitivities, while correlation effects act primarily as sealing factors that shift uncertainty magnitude.~~ (a) Selected-pair upwelling contrast $|\Delta L|$ versus correlated emissivity uncertainty. (b) $|\Delta L|$ versus minimum nonlinear emissivity sensitivity. (c) Minimum sensitivity versus correlated emissivity uncertainty. (d) Irradiance-driven~~uncertainty dominates, with~~ , emissivity-driven~~contributions remaining suppressed under Newton inversion~~, and total correlated T_s uncertainty components.

The ~~primary distinction between the two formulations is a systematic shift in magnitude that directly impacts the effective signal-to-noise ratio of the retrieval. The transition from independent to correlated error assumptions elevates the mean surface temperature uncertainty from K toK. This 41% increase in the mean error highlights the importance of accounting for covariance effects; ignoring these correlations would result in an overestimation of the signal to noise ratio and an overly optimistic view of the retrieval precision. Importantly, even with the inclusion of correlated errors, the emissivity-driven component () remains consistently suppressed relative to the irradiance-driven component (). This confirms that the adaptive conditioning within the Newton framework effectively regulates the emissivity-temperature coupling, ensuring that the retrieval remains stable even when the signal-to-noise ratio is challenged. The result is a robust retrieval system where the error budget is predictably scaled by measurement covariance without altering the fundamental physical pathways through which uncertainty propagates. This diagnostic transparency ensures that the resulting sub-kelvin error statistics are formally supported by the internal physics of the inversion~~first two relationships show that larger selected-pair upwelling contrast is generally associated with greater emissivity sensitivity and lower propagated emissivity uncertainty. The perfect rank anticorrelation between sensitivity and σ_ϵ follows directly from the mathematical structure of the local uncertainty formulation and is not treated as an independent validation statistic. Figure 6d extends the conditioning pathway to T_s through its irradiance- and emissivity-driven uncertainty components. These are propagated uncertainties; their empirical calibration is evaluated separately in Appendix C.

~~Table 3 reports the irradiance-driven and emissivity-driven components of surface temperature uncertainty under independent and correlated error assumptions, consistent with decomposition shown in Figure 11. These results indicate that the bounded surface temperature uncertainty of the Newton-based retrieval reflects intrinsic inversion conditioning and controlled emissivity-temperature coupling, rather than artifacts of idealized error assumptions or post-hoc noise suppression.~~

5.5 Field behaviour of retrieved broadband emissivity

~~**Table 3.** Surface temperature uncertainty components under independent and correlated error assumptions. Irradiance-driven and emissivity-driven contributions to surface temperature uncertainty for the Newton-based retrieval, illustrating their relative importance under stable inversion conditions~~Figure 7 shows retrieved broadband-emissivity distributions for the nine stations. All 632 production retrievals are included, with station medians and interquartile ranges. The distributions are interpreted descriptively rather than as field emissivity-validation errors because a common independent broadband-emissivity truth is not available for the complete field population.

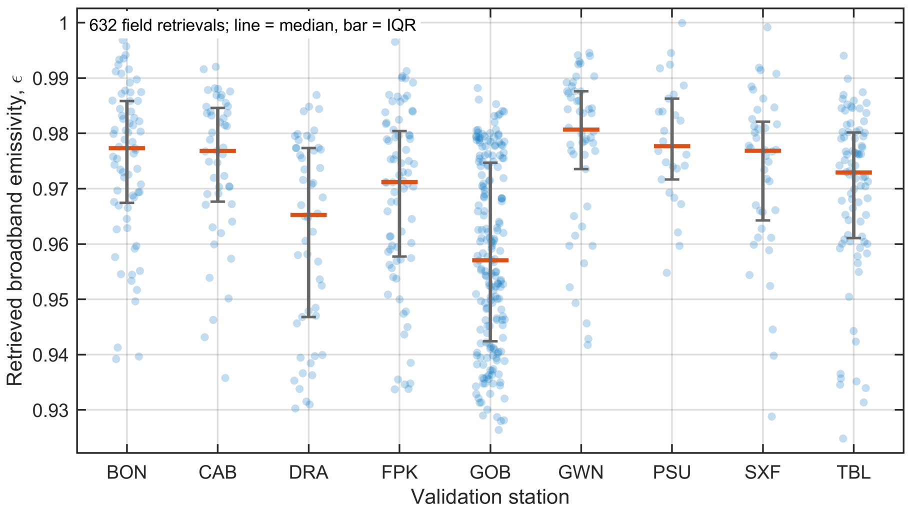

Figure 7. Station-wise distributions of retrieved broadband surface emissivity for the 632 field retrievals. Individual retrievals are shown together with the station median and interquartile range. The distributions characterize field retrieval behaviour and are not interpreted as direct emissivity-validation errors.

~~5.4 Surface temperature validation~~

~~This section evaluates the performance of the retrieved surface temperature against independent in-situ measurements to assess the physical realism and stability of the proposed retrieval framework. Validation is performed across a broad range of surface types, seasons, and atmospheric conditions, providing a stringent test of the combined emissivity-temperature inversion under both favorable and weakly conditioned irradiance regimes. The validation dataset used here was independently confirmed to be consistent with surface temperature values reported for the same SURFRAD stations and comparable atmospheric conditions (Zhang et al., 2016), ensuring that the present validation does not rely on unreferenced or duplicated benchmark data~~

5.6 Nine-station field surface-temperature validation

Figure 8 compares retrieved T_s with the ground-based validation-reference T_s for all 632 cases. Across the complete field population, the production retrieval has a bias of -0.162 K, MAE of 0.432 K, RMSE of 0.558 K, and $R^2 = 0.9984$.

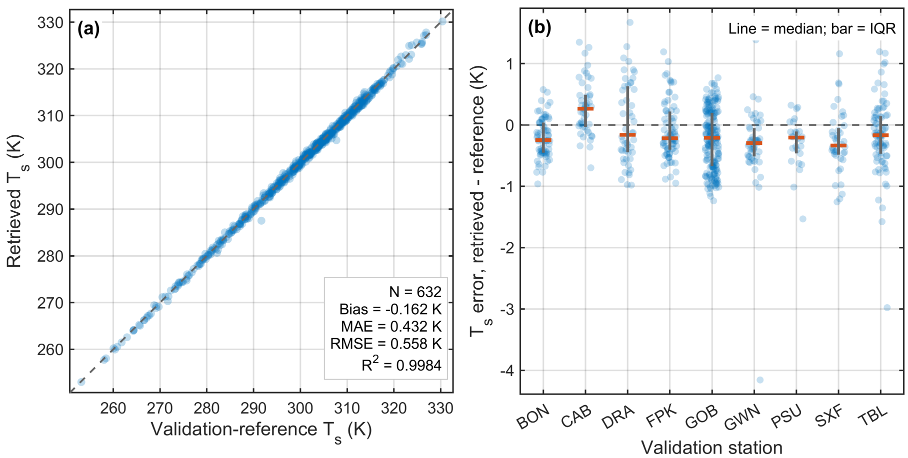

Figure 8. Field surface-temperature validation for all 632 retrievals. (a) Retrieved T_s versus ground-based validation-reference T_s for the nine stations, with the 1:1 relation shown for reference. (b) Station-wise distributions of signed error $T_{s,ret} - T_{s,ref}$.

~~**Figure 12.** Comparison of retrieved surface temperature against independent in-situ measurements across all sites and seasons. The one-to-one reference line, along with reportedand RMSE, indicates strong agreement and absence of systematic bias.~~

Table 2. Field surface-temperature validation performance by station and overall.

Station	Code	N	Bias (K)	SD (K)	MAE (K)	RMSE (K)	R²
Bondville	BON	69	-0.207	0.326	0.321	0.385	0.9992
Cabauw	CAB	47	0.284	0.445	0.397	0.524	0.9984
Desert Rock	DRA	50	0.020	0.664	0.569	0.658	0.9977
Fort Peck	FPK	75	-0.099	0.465	0.396	0.472	0.9993
Gobabeb	GOB	191	-0.238	0.481	0.443	0.536	0.9944
Goodwin Creek	GWN	50	-0.332	0.680	0.464	0.751	0.9942
Penn State	PSU	26	-0.289	0.410	0.372	0.495	0.9985
Sioux Falls	SXF	40	-0.275	0.505	0.465	0.570	0.9988
Table Mountain	TBL	84	-0.174	0.604	0.449	0.625	0.9979
All stations	**ALL**	**632**	**-0.162**	**0.534**	**0.432**	**0.558**	**0.9984**

The low overall bias indicates little systematic displacement relative to the field reference, while the MAE and RMSE show that the typical retrieval-reference difference remains well below 1 K. Station-wise values demonstrate that the aggregate result is assembled from distinct site populations rather than repeated observations from one homogeneous environment. The reference temperature nevertheless shares ground-based longwave measurements with the retrieval and is therefore not treated as fully independent radiometric truth.

5.7 Physics-based known-truth validation

The principal known-truth test is the G1 noiseless experiment shown in Fig. 9 and summarized in Table ~~4 summarizes validation statistics for both the Newton-based and linearized surface temperature retrievals relative to independent in-situ measurements, including retrieved temperature, bias, and absolute error. Across all cases, both approaches yield very similar mean bias and mean absolute error, indicating comparable average temperature accuracy. The distinction between the two methods is not in mean error magnitude, but in their numerical behaviour: the Newton-based retrieval maintains stable and bounded error characteristics across sites and atmospheric conditions, whereas the linearized formulation is more sensitive to irradiance conditioning. Overall, the close agreement with in-situ observations and consistency with formal uncertainty propagation demonstrate that reliable surface temperature retrieval can be achieved directly from broadband longwave irradiance measurements within the proposed diagnostic-driven framework~~3. Of the 6000 independently prescribed truth scenes, 5924 yield successful finite retrievals, corresponding to 98.73 %. All 6000 generated scenes remain in the success denominator.

~~**Table 4.** Validation statistics for Newton and linearized retrieved surface temperatures relative to in-situ measurements. Retrieved surface temperatures, bias and absolute error demonstrate improved and consistent performance of the Newton-bases retrieval across diverse sites and atmospheric conditions.~~

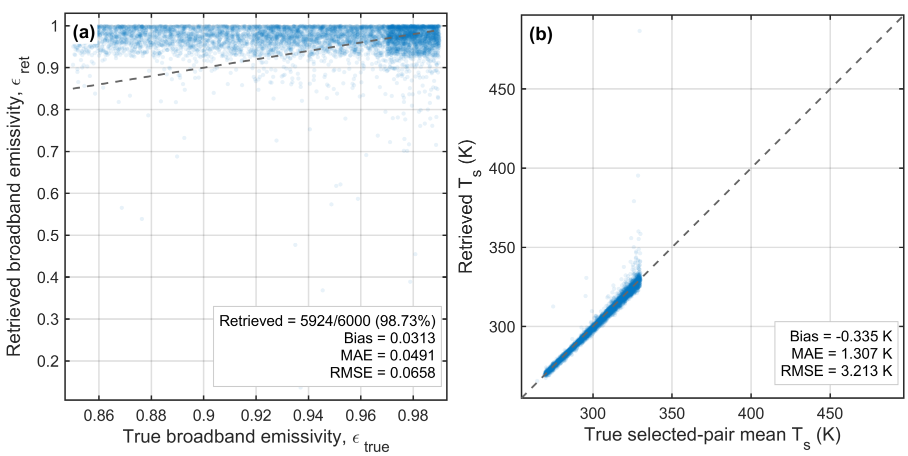

Figure 9. Physics-based known-truth validation for the G1 noiseless experiment. (a) Retrieved versus prescribed broadband emissivity for successful retrievals. (b) Retrieved T_s versus the true surface temperature corresponding to the selected production pair. The success denominator is all 6000 generated scenes; plotted error statistics use successful retrievals only.

~~5.5 Summary performance metrics~~

~~To provide a concise quantitative summary of retrieval performance, aggregate metrics were computed across all sites, seasons, and atmospheric conditions considered in this study. The retrieved surface temperature exhibits a small mean biasof -0.2693 K, indicating the absence of systemic over- or underestimation. The root mean square error (RMSE) is 0.5443 K, while the mean absolute error is 0.4663 K, demonstrating~~

Table 3. Physics-based known-truth validation for the G1 noiseless experiment, reported overall and by predefined emissivity regime.

True ε range	Generated scenes	Successful retrievals	Success (%)	ε bias	ε MAE	ε RMSE	T_s bias (K)	T_s MAE (K)	T_s RMSE (K)
Overall	**6000**	**5924**	**98.73**	**0.03129**	**0.04908**	**0.06578**	**-0.335**	**1.307**	**3.213**
0.85-0.92	2000	1967	98.35	0.08581	0.08778	0.09352	-1.754	2.043	2.522
0.92-0.97	2000	1976	98.80	0.02213	0.03575	0.05043	-0.058	1.001	4.337
0.97-0.99	2000	1981	99.05	-0.01370	0.02395	0.04148	0.797	0.882	2.407

Across successful retrievals, overall emissivity bias, MAE, and RMSE are 0.03129, 0.04908, and 0.06578, respectively. The corresponding T_s bias, MAE, and RMSE are -0.335, 1.307, and 3.213 K. Performance varies across emissivity regimes: the largest positive emissivity bias occurs in the lowest-emissivity interval, while the highest-emissivity interval has a smaller absolute bias and lower emissivity RMSE. The method therefore maintains high retrieval availability across $0.85 \le \epsilon_{true} \le 0.99$, but low-emissivity conditions remain the most demanding part of the tested retrieval space.

scenes. Detailed G1-G2 comparisons are retained in Appendix B because they quantify robustness to realistic measurement perturbations rather than constituting an additional independent validation population.

~~The emissivity retrieval exhibits similarly stable behavior. The mean Newton-retrieved emissivity uncertainty is 0.0077 under independent errors and 0.0109 when irradiance covariance is included, remaining well bounded across all cases. This result reinforces the conclusions of Sections 5.1-5.3: under well-conditioned Newton inversion, emissivity uncertainty remains physically interpretable and controlled by irradiance contrast and Jacobian strength. In contrast, the linearized emissivity, while often close in value, exhibits substantially larger and more variable uncertainty and is~~

~~therefore retained strictly as a diagnostic indicator rather than a physically meaningful estimate.~~

5.8 Integrated interpretation and limitations

The results support a conditioning pathway in which retrieval reliability arises from complementary controls rather than Newton behaviour alone. Temporal screening limits strong thermodynamic-state changes; irradiance identifiability requires surface-sensitive contrast; progressive population analysis requires sufficient independent information and centre stability; physical-state diagnostics determine reciprocal applicability; and Newton refinement solves the resulting nonlinear emissivity equation.

~~Overall, these summary metrics confirm that the proposed retrievalframework achieves reliable surface temperature estimation not only in terms of accuracy, but also in terms of numerical stability, conditioning, and uncertainty control. The close correspondence between observed validation error and the correlated, irradiance-driven uncertainty demonstrates that surface temperature errors are consistent with expected measurement limitations and are not dominated by unsuppressed emissivity-driven amplification. This agreement between diagnostic uncertainty estimates and validation performance provides strong evidence for the physical reliability and robustness of the derived surface temperature and emissivity products~~The field and synthetic experiments provide complementary evidence. The field observations retain real instrument behaviour, atmospheric variability, temporal variability, and surface heterogeneity, but the validation-reference T_s shares longwave radiometric information with the retrieval. The synthetic experiment provides independently prescribed emissivity and temperature truth but necessarily represents a controlled physical model of the observed environment. Confidence in the retrieval therefore derives from the consistency of the two lines of evidence rather than from either experiment alone.

Two further limitations are important. First, the conditioning and Newton diagnostics describe the screened production population and should not be extrapolated to arbitrary longwave temporal pairs. Second, propagated uncertainty quantifies local measurement and emissivity sensitivity but is not automatically a calibrated confidence interval. Known-truth uncertainty coverage is therefore evaluated separately in Appendix C. The synthetic validation was evaluated without subsequent retuning of production thresholds, pair-selection rules, reciprocal-state logic, or uncertainty parameters using the synthetic outcomes.

6 Conclusions

This study presents a conditioning-controlled ~~retrieval framework for estimating~~ framework for retrieving broadband surface emissivity and land surface temperature directly from paired ground-based upwelling and downwelling longwave irradiance measurements. ~~Using high-temporal-resolution SURFRAD observations as a measurement testbed, the retrieval is formulated as a nonlinear inverse problem in which numerical conditioning, parameter observability, and uncertainty structure are treated as intrinsic components of the measurement interpretation rather than secondary numerical details. In this respect, the approach aligns explicitly with~~

~~inverse-problem theory (Rodgers, 2000; Tarantola, 2005) by emphasizing diagnostic consistency, Jacobian-controlled stability, and physically interpretable uncertainty propagation in addition to conventional accuracy metrics~~The inverse problem is treated as an information-limited radiometric retrieval in which thermal-state consistency, numerical admissibility, irradiance identifiability, information sufficiency, physical-state applicability, nonlinear refinement, and uncertainty propagation are incorporated explicitly into the retrieval workflow. The framework therefore addresses observability before nonlinear inversion rather than relying on convergence behaviour alone as evidence of retrieval reliability.

A ~~central result of this work is the demonstration that broadband emissivity and surface temperatureretrieval are fundamentally governed by irradiance contrastand inversion conditioning. Although linearized emissivity formulations may yield values numerically close to nonlinear solutions, their associated uncertainty structure becomes ill-conditioned under common observational regimes characterized by strong atmospheric downwelling irradiance and weak temporal contrast. The divergence of linearized emissivity uncertainty is shown to be a structural consequence of the linear approximation when the signal-to-noise ratio of the irradiance contrast becomes insufficient to support stable inversion.~~ population-based progressive temporal search identifies production pairs from the available local observations. Candidate pairs are screened for quasi-steady apparent surface temperature, numerical and physical admissibility, and resolvable surface-sensitive irradiance contrast. Their local information content is then evaluated using propagated candidate uncertainty together with marginalized emissivity information, while the final production pair is selected without ranking candidates according to their emissivity value. Among the 632 usable field datasets, 628 satisfied the stable-centre selection criterion and only four required the prescribed fallback pathway; the median selected-pair separation was 3 min.

The framework also incorporates an explicit physical-state treatment of the reciprocal emissivity formulations. Reciprocal transformation is applied conditionally according to the radiative state surrounding the selected observation pair rather than as a universal algebraic correction. The resulting state-conditioned emissivity provides the initial state for the fixed eight-update Newton-Raphson refinement. Numerical residuals and local sensitivities are consequently interpreted within a population that has already passed the preceding physical and information-based conditioning stages.

~~In contrast, the Newton-based formulation enforces the full nonlinear irradiance balance and explicitly accounts for emissivity temperature coupling. Emissivity uncertainty is governed by the inversion Jacobian and therefore remains bounded whenever emissivity is observable. As irradiance contrast weakens, uncertainty increases smoothly and diagnostically rather than catastrophically, providing physically interpretable information regarding retrieval reliability. This bounded behavior confirms that inversion stability is controlled by conditioning diagnostics rather than by numerical artifacts~~Field validation comprised 637 source datasets from nine SURFRAD and BSRN stations spanning vegetated, mixed, and bare/desert environments. Five datasets lacked the required finite initial validation-pair irradiances, leaving 632 usable cases, all of which produced final finite retrievals. Across this population, retrieved T_s had an overall bias of -0.162 K, MAE of 0.432 K, RMSE of 0.558 K, and $R^2 = 0.9984$ relative to the ground-based validation-reference temperature.

~~The surface temperature retrieval benefits significantly from the robust characterization of emissivity within the Newton-based framework. By explicitly decomposing temperature uncertainty into emissivity-driven and irradiance-driven components,~~ Direct broadband-emissivity validation was provided by the ~~analysis clarifies the physical pathways through which uncertainty propagates. Contrary to typical assumptions in low-signal regimes, irradiance-driven uncertainty remains the dominant contributor under weak irradiance contrast, reflecting the sensitivity of the retrieval to the signal-to-noise ratio. While emissivity-driven uncertainty remains a secondary component, its relative importance increases slightly as irradiance contrast improves. Adaptive temporal pairing enhances surface temperatureprecision indirectly by improving emissivity conditioning, thereby stabilizing the inversion without altering the baseline irradiance uncertainty. Validation against independent in-situ measurements confirms this consistency, with sub-Kelvin error statistics that align with the formally propagated, correlated uncertainty.~~ complementary physics-based synthetic experiment. Six thousand truth scenes were generated, with exactly 2000 scenes in each of the predefined emissivity regimes $0.85 \leq \epsilon < 0.92$, $0.92 \leq \epsilon < 0.97$, and $0.97 \leq \epsilon \leq 0.99$. In the noiseless known-truth experiment, 5924 of 6000 scenes were successfully retrieved (98.73 %). Across successful retrievals, the overall emissivity bias, MAE, and RMSE were 0.0313, 0.0491, and 0.0658, respectively, while the corresponding T_s bias, MAE, and RMSE were -0.335, 1.307, and 3.213 K. Retrieval performance varied across emissivity regimes, with the lowest-emissivity interval showing the largest positive emissivity bias and the highest emissivity RMSE.

~~*From Diagnostic Framework to Operational Efficiency*: The selection of a fixed, maximumfor the iterative solver was a deliberate choice for this validation study, allowing for transparent diagnosis of the Jacobian and convergence order. For operational implementation, this is superseded by a dynamic stopping criterion: (1)Monitoring the Jacobian magnitude, to halt the retrieval if it approaches an ill-conditioned regime (typically); and (2) terminating the Newton iteration when the change in emissivity is less than a tolerance defined by the formally propagated emissivity uncertainty. This transition ensures the algorithm remains both scientifically transparent and computationally efficient.~~ The field and synthetic experiments provide complementary evidence. The field observations contain real atmospheric variability, instrument behaviour, temporal variability, and surface heterogeneity, but the validation-reference temperature shares ground-based longwave radiometric information with the retrieval. The synthetic experiment provides independently prescribed emissivity and temperature truth but necessarily represents a controlled forward model of the observed environment. Their combined interpretation therefore provides stronger evidence than either experiment alone.

~~*Extensibility of the Framework*: Although the current study's validation is rigorously constrained to surface-based observations where atmospheric transmittance and emission terms are limited to the downwelling path, the core of the proposed diagnostic framework is mathematically general. The fundamental methodology-Newton inversion, Jacobian based conditioning diagnostics, and uncertainty decomposition, can be directly applied to more complex radiative transfer problems, such as those encountered in satellite bases LST retrieval~~ Several limitations remain. The field temperature reference is not independent of all longwave measurements used by the retrieval. The synthetic experiment reproduces empirically grounded short-term radiative forcing but cannot represent every unmodelled process or representativeness error present at real field sites. Retrieval errors also increase in portions of the lower-emissivity truth space, indicating that weak-information conditions remain challenging. Further work should focus on validation against independent broadband emissivity and surface-temperature references, extension to additional low-emissivity surface types and radiative regimes, and continued evaluation of uncertainty calibration under weak-information conditions.

Overall, the main contribution is an integrated retrieval architecture in which observability is assessed before inversion, physical applicability is treated explicitly, numerical refinement is diagnosed rather than assumed, and validation combines real-field performance with independently prescribed known truth. The results demonstrate that broadband emissivity and land surface temperature can be jointly retrieved from high-temporal-resolution paired longwave irradiance measurements without requiring externally prescribed emissivity as an input to the retrieval itself.

Appendix A: Workflow-stage accounting

Appendix A provides the detailed field sample and candidate-pair accounting underlying the compact audit shown in Fig. 2. The accounting is read-only and does not alter the retrieval.

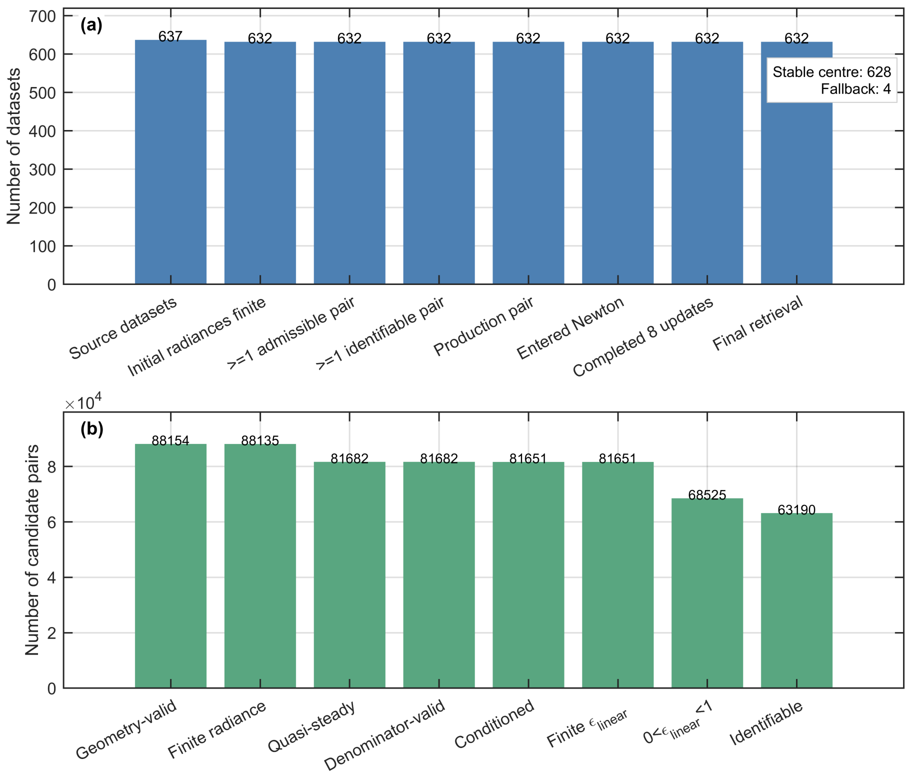

Figure A1. Workflow-stage accounting for the field dataset. (a) Scene-level progression from source datasets to final retrievals. (b) Candidate-pair retention through the physical, numerical, and irradiance-identifiability screening stages.

~~Extending the framework only requires modifying the irradiance model (Equation 1) to incorporate the full atmospheric transmittance and upwelling emission terms, which introduce additional, but treatable, complexity into the Jacobian structure. The key finding, that LST retrieval reliability is governed by the Jacobian of the inversion, remains universally valid regardless of the specific radiative transfer terms included. Future work will focus on integrating a full radiative transfer model into the Jacobian, to demonstrate the framework's applicability to high-altitude or space radiometric~~

Table A1. Detailed overall field workflow-stage accounting.

Audit stage	Count
Source files seen	637
Files with validation-time constraint	637
Files with valid data record/layout	637
Files with finite initial validation-pair irradiances	632
Scenes with >=1 admissible linear-epsilon pair	632
Scenes with >=1 irradiance-identifiable pair	632

Audit stage	Count
Scenes selected by stable-centre criterion	628
Scenes selected through fallback	4
Scenes with finite production pair	632
Scenes entering Newton-Raphson	632
Scenes with >=1 valid Newton update	632
Scenes completing 8 valid Newton updates	632
Scenes with invalid Newton break	0
Final finite retrievals	632
PAIR COUNT: geometry-valid	88154
PAIR COUNT: finite-irradiance	88135
PAIR COUNT: quasi-steady	81682
PAIR COUNT: denominator-valid	81682
PAIR COUNT: conditioned	81651
PAIR COUNT: finite linear epsilon	81651
PAIR COUNT: 0<linear epsilon<1	68525
PAIR COUNT: irradiance-identifiable	63190

~~By explicitly linking emissivity observability, numerical conditioning, adaptive temporal pairing, and formal uncertainty propagation, this study establishes a transparent and reproducible methodology for extracting physically reliable broadband surface temperature and emissivity estimates from ground-based longwave irradiance measurements. The framework complements existing validation efforts by embedding diagnostic conditioning control directly within the retrieval design, thereby strengthening the interpretability and physical reliability of measurement-based~~

Table A2. Station-wise field workflow accounting.

Site	Source	Initial finite	Admissible	Identifiable	Stable	Fallback	Prod. pair	8 updates	Final
BON	70	69	69	69	69	0	69	69	69
CAB	48	47	47	47	47	0	47	47	47
DRA	50	50	50	50	50	0	50	50	50
FPK	75	75	75	75	75	0	75	75	75
GOB	194	191	191	191	190	1	191	191	191
GWN	50	50	50	50	49	1	50	50	50
PSU	26	26	26	26	26	0	26	26	26
SXF	40	40	40	40	39	1	40	40	40
TBL	84	84	84	84	83	1	84	84	84
ALL	**637**	**632**	**632**	**632**	**628**	**4**	**632**	**632**	**632**

Appendix B: Synthetic realism and production-noise robustness

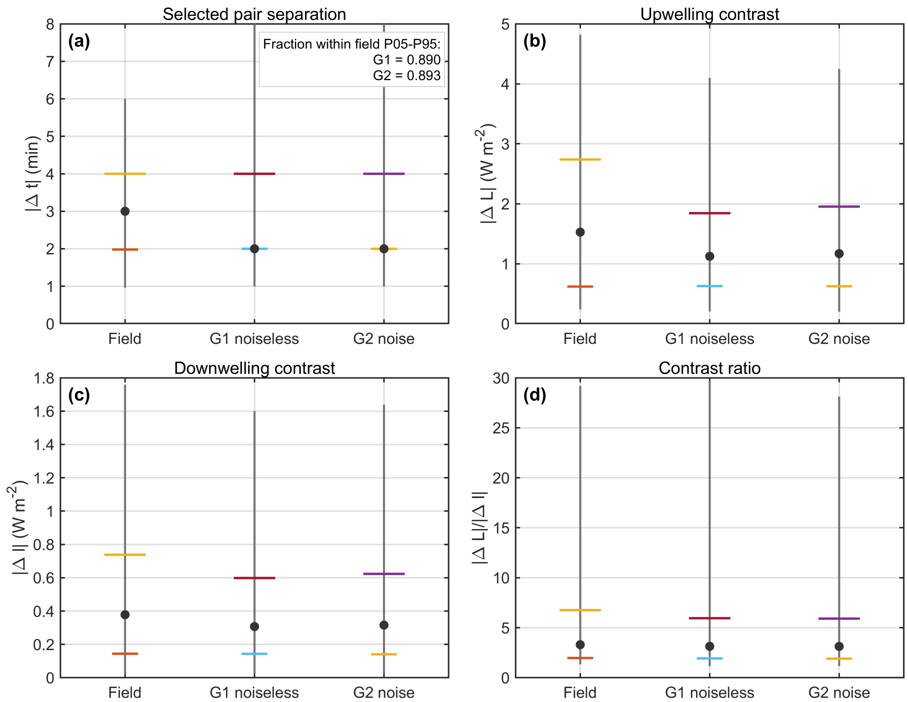

Figure B1. Field-versus-synthetic selected-pair geometry. Field quantiles are compared with G1 noiseless and G2 production-noise synthetic quantiles for selected-pair separation and the principal longwave contrast variables.

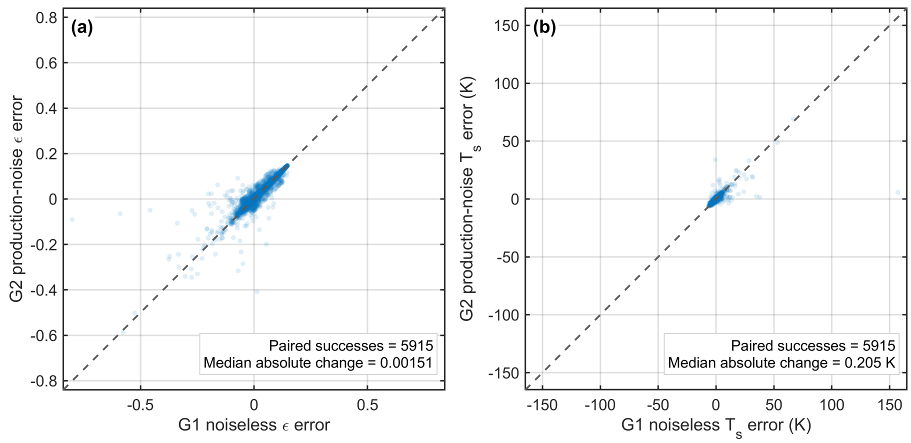

Figure B2. Paired G1-versus-G2 production-noise robustness for the same prescribed truth scenes. The panels compare the change in emissivity error and the change in T_s error when the pre-specified production-noise model is added before preprocessing.

Table B1. Synthetic performance for G1 noiseless and G2 production-noise experiments, reported overall and by predefined emissivity regime.

Experiment	True ε range	Generated	Successful	Success (%)	ε bias	ε MAE	ε RMSE	T_s bias (K)	T_s MAE (K)	T_s RMSE (K)
G1 noiseless	Overall	6000	5924	98.73	0.03129	0.04908	0.06578	-0.335	1.307	3.213
G1 noiseless	0.85-0.92	2000	1967	98.35	0.08581	0.08778	0.09352	-1.754	2.043	2.522
G1 noiseless	0.92-0.97	2000	1976	98.80	0.02213	0.03575	0.05043	-0.058	1.001	4.337
G1 noiseless	0.97-0.99	2000	1981	99.05	-0.01370	0.02395	0.04148	0.797	0.882	2.407
G2 production noise	Overall	6000	5939	98.98	0.03181	0.04885	0.06568	-0.376	1.311	2.712
G2 production noise	0.85-0.92	2000	1970	98.50	0.08604	0.08810	0.09380	-1.763	2.066	2.621
G2 production noise	0.92-0.97	2000	1981	99.05	0.02253	0.03573	0.05025	-0.143	0.953	2.744
G2 production noise	0.97-0.99	2000	1988	99.40	-0.01269	0.02304	0.04067	0.766	0.920	2.770

Appendix C: Detailed emissivity-range and uncertainty diagnostics

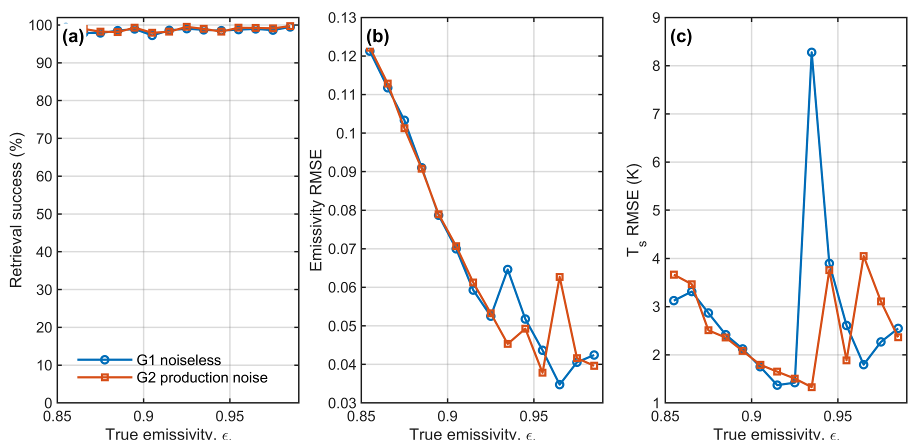

Table C1. Synthetic uncertainty calibration and nominal one-sigma coverage for emissivity and T_s.

Experiment	True ε range	N ε	ε within 1σ (%)	Median |zε|	N T_s	T_s within 1σ (%)	Median |zT_s|
G1 noiseless	Overall	5924	25.9	3.119	5924	40.2	1.472
G1 noiseless	0.85-0.92	1967	4.5	7.138	1967	10.9	3.533
G1 noiseless	0.92-0.97	1976	22.1	2.270	1976	46.9	1.090
G1 noiseless	0.97-0.99	1981	51.0	0.949	1981	62.7	0.500
G2 production noise	Overall	5939	25.9	3.089	5939	38.7	1.517
G2 production noise	0.85-0.92	1970	4.7	7.186	1970	11.7	3.615
G2 production noise	0.92-0.97	1981	22.2	2.323	1981	45.0	1.130
G2 production noise	0.97-0.99	1988	50.5	0.968	1988	59.3	0.760

Competing interests

The author ~~declare no conflicts of interest~~declares that there are no competing interests.

Acknowledgements

The author gratefully ~~acknowledge the U.S. Department of Energy Atmospheric Radiation Measurement (ARM) program for providing the Surface Radiation Network (SURFRAD) dataused in this study. The high quality, long-term broadband irradiance measurements made available through SURFRAD were essential for the development and evaluation of the retrieval methodology presented in this~~ acknowledges the organizations and data providers that maintain the SURFRAD and BSRN radiation records used in this study, and Mohannad Loho of Damascus University for providing part of the SURFRAD validation data. work.

Financial support

This research received no external funding.

References

Aster, R. C., Borchers, B., and Thurber, C. H.: Parameter Estimation and Inverse Problems, 3rd ed., Elsevier Academic Press, Cambridge, MA, USA, 2019.

Augustine, J. A., DeLuisi, J. J., and Long, C. N.: SURFRAD—A national surface radiation budget network for atmospheric research, Bull. Am. Meteorol. Soc., 81, 2341–2357, https://doi.org/10.1175/1520-0477(2000)081<2341:SANSRB>2.3.CO;2, 2000.

Augustine, J. A., Hodges, G. B., Cornwall, C. R., Michalsky, J. J., and Medina, C. I.: An update on SURFRAD—The GCOS surface radiation budget network for the continental United States, J. Atmos. Ocean. Technol., 22, 1460–1472, https://doi.org/10.1175/JTECH1806.1, 2005.

Dash, P., Göttsche, F.-M., Olesen, F.-S., and Fischer, H.: Land surface temperature and emissivity estimation from passive sensor data: Theory and practice; current trends, Int. J. Remote Sens., 23, 2563–2594, ~~,~~ https://doi.org/10.1080/01431160110115041, 2002.

~~Dennis, J. E. and Schnabel, R. B.:Numerical Methods for Unconstrained Optimization and Nonlinear Equations, Society for Industrial and Applied Mathematics, Philadelphia, PA, USA, 1996.~~

Gillespie, A. R., Rokugawa, S., Matsunaga, T., Cothern, J. S., Hook, S. J., and Kahle, A. B.: A temperature and emissivity separation algorithm for Advanced Spaceborne Thermal Emission and Reflection Radiometer (ASTER) images, IEEE Trans. Geosci. Remote Sens., 36, 1113–1126, https://doi.org/10.1109/36.700995, 1998.

Hulley, G. C. and Hook, S. J.: Generating consistent land surface temperature and emissivity products between ASTER and MODIS data for Earth science research, IEEE Trans. Geosci. Remote Sens., 49, 1304–1315, https://doi.org/10.1109/TGRS.2010.2063034, 2011.

Li, S., Yu, Y., Sun, D., Tarpley, D., Zhan, X., and Chiu, L.: Evaluation of 10-year AQUA/MODIS land surface temperature with SURFRAD observations, Int. J. Remote Sens., 35, 830–856, https://doi.org/10.1080/01431161.2013.873149, 2014.

Li, Z.-L., Li, L., Tang, B.-H., and Cribb, M. C.: A review of methods for retrieving land surface emissivity from space, Remote Sens. Environ., 231, 111199, https://doi.org/10.1016/j.rse.2019.111199, 2019.

Li, Z.-L., Tang, B.-H., Wu, H., Ren, H., Yan, G., Wan, Z., Trigo, I. F., and Sobrino, J. A.: Satellite-derived land surface temperature: Current status and perspectives, Remote Sens. Environ., 131, 14–37, https://doi.org/10.1016/j.rse.2012.12.008, 2013.

Li, Z.-L., Wu, H., Duan, S.-B., Zhao, W., Ren, H., Liu, X., Leng, P., Tang, R., Ye, X., Zhu, J., Sun, Y., Si, M., Liu, M., Li, J., Zhang, X., Shang, G., Tang, B.-H., Yan, G., and Zhou, C.: Satellite remote sensing of global land surface temperature: Definition, methods, products, and applications, Rev. Geophys., 61, e2022RG000777, https://doi.org/10.1029/2022RG000777, 2023.

Menke, W.: Geophysical Data Analysis: Discrete Inverse Theory, 3rd ed., Academic Press, Burlington, MA, USA, 2012.

Nocedal, J. and Wright, S. J.: Numerical Optimization, Springer, New York, NY, USA, 2006.

~~Norman, J. M., Kustas, W. P., and Humes, K. S.: A two-source approach for estimating soil and vegetation energy fluxes from observations of directional radiometric surface temperature, Agric. For. Meteorol., 77, 263–293, https://doi.org/10.1016/0168-1923(95)02265-Y, 1995.~~

Ortega, J. M. and Rheinboldt, W. C.: Iterative Solution of Nonlinear Equations in Several Variables, Society for Industrial and Applied Mathematics, Philadelphia, PA, USA, https://doi.org/10.1137/1.9780898719468, 2000.

Rodgers, C. D.: Inverse Methods for Atmospheric Sounding: Theory and Practice, World Scientific, Singapore, https://doi.org/10.1142/3171, 2000.

Tarantola, A.: Inverse Problem Theory and Methods for Model Parameter Estimation, Society for Industrial and Applied Mathematics, Philadelphia, PA, USA, https://doi.org/10.1137/1.9780898717921, 2005.

Wan, Z.: New refinements and validation of the collection-6 MODIS land-surface temperature/emissivity product, Remote Sens. Environ., 140, 36–45, https://doi.org/10.1016/j.rse.2013.08.027, 2014.

Wang, M., Zhang, Z., Hu, T., and Liu, X.: A practical single-channel algorithm for land surface temperature retrieval: Application to Landsat series data, J. Geophys. Res. Atmos., 124, 299–316, https://doi.org/10.1029/2018JD029330, 2019.

Zhang, Z., He, G., Wang, M., Long, T., Wang, G., and Zhang, X.: Validation of the generalized single-channel algorithm using Landsat 8 imagery and SURFRAD ground measurements, Remote Sens. Lett., 7, 810–816, https://doi.org/10.1080/2150704X.2016.1190475, 2016.